Multi-timescale systems and fast-slow analysis

Richard Bertram [a,*], Jonathan E. Rubin [b]

[a] *Department of Mathematics and Programs in Neuroscience and Molecular Biophysics Florida State University, Florida State University, Tallahassee, FL, United States*
[b] *Department of Mathematics, University of Pittsburgh, Pittsburgh, PA, United States*

A R T I C L E   I N F O

A B S T R A C T

Mathematical models of biological systems often have components that vary on different timescales. This multi-timescale character can lead to problems when doing computer simulations, which can require a great deal of computer time so that the components that change on the fastest time scale can be resolved. Mathematical analysis of these multi-timescale systems can be greatly simplified by partitioning them into subsystems that evolve on different time scales. The subsystems are then analyzed semi-independently, using a technique called fast-slow analysis. In this review we describe the fast-slow analysis technique and apply it to relaxation oscillations, neuronal bursting oscillations, canard oscillations, and mixed-mode oscillations. Although these examples all involve neural systems, the technique can and has been applied to other biological, chemical, and physical systems. It is a powerful analysis method that will become even more useful in the future as new experimental techniques push forward the complexity of biological models.

© 2016 Elsevier Inc. All rights reserved.

1. Introduction

Biological systems often feature interacting components that vary on disparate timescales. For example, changes in a cell's environment trigger variations in protein levels through a sequence of protein–protein interactions, leading to changes in gene transcription, followed by translation and often post-translational modification. This process may be followed by translocation of proteins, such as ion channels or hormone receptors, into the cell's plasma membrane, which allows the cell to respond appropriately to its environment. This whole process can take hours, even though the fastest components (such as protein–protein interactions) occur on the timescale of seconds. An even wider gap exists between rapid cellular events such as neuronal electrical activity and much slower circadian rhythms coordinated through the suprachiasmatic nucleus of the hypothalamus and involving rhythms in gene expression.

Such examples are problematic for computer simulations of mathematical models, which are computationally expensive if changes at the fastest timescale are resolved. Fortunately, there are specialized mathematical techniques that can be applied to analyze the behavior of systems in which the separation of timescales is sufficiently large. There is a substantial literature on multiple-scale asymptotic analysis of systems with timescale separation (e.g., [48]). Alternatively, one can employ geometric methods often denoted as *fast-slow analysis* to simplify the investigation of the system by breaking it into two or more reduced subsystems that are more tractable than the full model. There are two primary goals of this article. The first is to provide an overview of some fast-slow analysis techniques. The second is to illustrate some behaviors that come about in multi-timescale systems and that are best understood from the viewpoint of fast-slow analysis. We use examples that involve the dynamics of electrically excitable cells, but other studies of multiscale dynamics and their analysis focus on chemically reacting systems, intracellular calcium dynamics, ecology, climate dynamics, and other application areas (e.g., [45,55,67,74,75,77]).

A system of ordinary differential equations that evolves on two timescales can be formally written as

$$\frac{d\vec{x}}{dt} = F(\vec{x}, \vec{y}) \tag{1}$$

$$\frac{d\vec{y}}{dt} = \epsilon G(\vec{x}, \vec{y}) \tag{2}$$

where $\epsilon > 0$ is small. The *fast variables* $\vec{x}$ evolve on a faster timescale than the *slow variables* $\vec{y}$, and we can define a corresponding *fast subsystem* $d\vec{x}/dt = F(\vec{x}, \vec{y})$, with $\vec{y}$ as parameters, and *slow subsystem* $d\vec{y}/d\tau = G(\vec{x}_F(\vec{y}), \vec{y})$, where $\vec{x}_F$ is defined from $F(\vec{x}, \vec{y}) = 0$ and $\tau = \epsilon t$ corresponds to a slow timescale. The dimensionality of the two subsystems differs among applications,

* Corresponding author. Fax: +1 850 644 4053.
  E-mail address: bertram@math.fsu.edu (R. Bertram).

but the general approach of fast-slow analysis is to treat the subsystems separately. The idea underlying this splitting into subsystems is that from a general initial condition, the system will be governed by the fast subsystem and will settle to the neighborhood of a fast subsystem attractor, where $F = 0$, that is parameterized by $\bar{y}$. Within this neighborhood, the system will evolve slowly, governed by the slow subsystem, unless a boundary of the attractor is reached and the fast subsystem takes over again. Fast-slow analysis is often employed to study relaxation oscillations, such as those that occur in the van der Pol oscillator with strong damping [96,102]. Here, the original second-order nonlinear differential equation can be converted into two first-order differential equations, yielding a single fast variable and a single slow variable. This system has been used to describe a heartbeat [103], and similar planar systems have been used to describe electrical impulses in neurons [40,41,68], intracellular calcium dynamics in a neuron [34], and hourly hormone pulses [105].

More than twenty years after Richard FitzHugh used fast-slow analysis to analyze what is now called the FitzHugh–Nagumo model, John Rinzel adapted the fast-slow analysis technique to understand the dynamics underlying bursting in neurons and pancreatic β-cells [4,78,79,82,83]. *Bursting* is characterized by active episodes of rapid electrical oscillations (also called impulses, spikes, or action potentials) separated by quiescent or silent phases, repeated periodically. It is ubiquitous in neurons and endocrine cells [24,95] and has been shown to be more effective at evoking neurotransmitter and hormone secretion than continuous trains of action potentials [61,104]. The technique developed by Rinzel explains such things as the existence of the bursting oscillation, patterns in interspike interval duration, the duty cycle (the fraction of the period during which the system is spiking), transitions between bursting and continuous spiking, and the roles that various ionic currents play in the bursting pattern. In addition, the bifurcations of the fast subsystem are useful for categorizing bursts; the bifurcation responsible for the transition from silent to active phase and that associated with the transition from active to silent phase determine the type of bursting oscillation [7,51,80]. Fast-slow analysis is now regularly used in the analysis of bursting oscillations, and in the first portion of this article we describe the method and give some applications.

In addition to relaxation and bursting oscillations, one other class of oscillations that comes up in fast-slow systems is called *mixed-mode oscillations* (MMOs). These consist of small-amplitude oscillations mixed with large-amplitude oscillations, often repeated periodically. MMOs have been identified and analyzed using mathematical models in chemically reacting systems [55,75], voltage dynamics of neurons [10,30,33,44,50,62,65,85–87] and electrically excitable pituitary cells [107,108], intracellular calcium dynamics [45], and elsewhere [67]. The small-amplitude oscillations are often due to *canards*, which are orbits that follow a curve or sheet of attracting equilibria as well as a portion of a repelling curve/sheet of equilibria of the fast subsystem. Though originally studied in a system with one fast and one slow variable [31,37], canards can be generic in systems with two or more slow variables, so they occur over much larger regions of parameter space in the latter case (see [29] for an excellent review of canards and MMOs). In the context of neurons, the small oscillations are subthreshold voltage oscillations, while the large oscillations are action potentials. Thus, the canard orbits have the effect of increasing the time between spikes, and thereby reducing the spike frequency [87]. In electrically excitable pituitary cells the canard orbits themselves are the "spikes", which are typically quite small, and the large oscillations are repolarizations that occur between bursts [106]. In the second portion of this article we illustrate how canard orbits come about in the context of MMOs and discuss some applications of MMOs in electrically excitable neurons and pituitary cells.

We note that when the first issue of *Mathematical Biosciences* was published in 1967, little of what we discuss in this article had been discovered. Relaxation oscillations had been around for half a century, but bursting oscillations, canards, and mixed-mode oscillations were all in the future. The future is now!

2. Relaxation oscillations and canards in a planar fast-slow system

Planar systems allow us to illustrate how the basic interplay between fast and slow variables can give rise to a characteristic form of oscillations. Furthermore, they provide a clear view of transitional phenomena that arise as a parameter is varied such that a bifurcation from steady state to oscillatory behavior occurs. We will illustrate these points with a single model system, noting that qualitatively similar phenomena occur in other systems with similar mathematical structure.

As mentioned above, the van der Pol oscillator with strong damping is the canonical fast-slow system with a single fast and a single slow variable. For purposes of continuity with later sections, we begin with a fast-slow system that describes membrane potential oscillations in an electrically active cell and that captures the dynamic features of the van der Pol oscillator. This is based on the "s-model" for pancreatic β cells [91]. This model has a variable for the membrane potential or voltage (V), an *activation variable* for the fraction of activated delayed rectifier K$^+$ channels (n), and an activation variable for the fraction of activated K$^+$ channels of another type (s). These latter K$^+$ channels could be Ca^{2+}-activated K$^+$ channels, for example. The dynamics of the variables are described by the following differential equations:

$$\frac{dV}{dt} = -(I_{Ca} + I_{Kdr} + I_{KATP} + I_{Ks} + I_L)/C_m \tag{3}$$

$$\frac{ds}{dt} = \frac{s_\infty(V) - s}{\tau_s} \ . \tag{4}$$

The change of voltage depends on several ionic currents reflecting ion flux through different ion channels. The V-dependent Ca^{2+} current, I_{Ca}, is an inward current that is responsible for the upstroke of a spike. It is similar to the Na$^+$ current in neurons, although its inactivation is much slower and is not included in the s-model. (A Na$^+$ current is also not included, since Na$^+$ channels are inactivated in mouse β cells.) Like the Na$^+$ current, the Ca^{2+} current activates very rapidly, and in the s-model it is assumed to adjust instantaneously to changes in V. This is called a *quasi-equilibrium* or *quasi-steady-state approximation* and is often used in multi-timescale models [42]. Using this assumption, the Ca^{2+} current is $I_{Ca} = g_{Ca}m_\infty(V)(V - V_{Ca})$, where g_{Ca} is the maximum conductance (the conductance when all channels are activated), $V - V_{Ca}$ is the *driving force* that powers ion flux through open channels, and $m_\infty(V)$ is the equilibrium activation function, given by the increasing sigmoid function

$$m_\infty(V) = \frac{1}{1 + e^{\frac{v_m - V}{s_m}}} \ . \tag{5}$$

This function, which ranges from 0 to 1, is half-maximal at $V = v_m$ and the steepness of the curve is determined by s_m (the curve is steeper when s_m is small). The other inward or depolarizing current is I_L, which is a constant-conductance leakage current that groups together the effects of various ion-specific flows and takes the form $I_L = g_L(V - V_L)$.

Model (3) and (4) includes three outward or hyperpolarizing currents, all carried by K$^+$. The first, I_{Kdr}, is the standard delayed rectifier that is responsible for the downstroke of an action potential. Activation of this current is considerably slower than that of the Ca^{2+} current (otherwise there would be no spike), so the

Table 1
Parameters for the planar fast-slow system, based on [91].

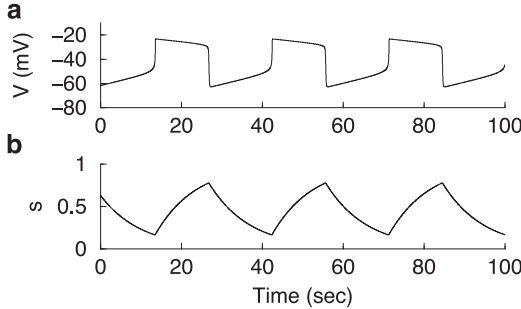|		
$g_{Ca} = 280$ pS	$g_L = 25$ pS	$g_{Kdr} = 1300$ pS
$g_s = 35$ pS	$g_{KATP} = 13$ pS	$C_m = 4524$ fF
$V_K = -80$ mV	$V_{Ca} = 100$ mV	$V_L = -40$ mV
$v_m = -22$ mV	$v_n = -9$ mV	v_s varies
$s_m = 7.5$ mV	$s_n = 10$ mV	$s_s = 0.5$ mV

Fig. 1. Relaxation oscillations produced by a planar fast-slow system. **(A)** The fast variable V has a square wave time course. **(B)** The slow variable s has a sawtooth time course. Here, $v_s = -40$ mV.

quasi-equilibrium approximation is not typically used in the s-model. However, we apply the approximation here so as to maintain a planar system. This has the effect of eliminating the spikes, but as we shall see it still allows for relaxation oscillations. With the quasi-equilibrium approximation, the delayed rectifier current is $I_{Kdr} = g_{Kdr}n_\infty(V)(V - V_K)$. The n equilibrium function is given by

$$n_\infty(V) = \frac{1}{1 + e^{\frac{v_n - V}{s_n}}} \quad . \tag{6}$$

The second K$^+$ current, I_{Ks}, reflects K$^+$ flux through a separate set of ion channels that activate on a slow timescale. This timescale is set by the parameter τ_s, which we choose so that s changes much more slowly than V. The current is given by $I_s = g_s s(V - V_K)$ and the s dynamics are described by Eq. (4), where the s_∞ function is

$$s_\infty(V) = \frac{1}{1 + e^{\frac{v_s - V}{s_s}}} \quad . \tag{7}$$

The third hyperpolarizing current, I_{KATP}, reflects K$^+$ flux through ATP-sensitive K$^+$ channels. These channels respond to the adenosine triphosphate (ATP) that is produced through glucose metabolism, and the expression of the channels in β cells allows them to respond to the blood glucose level [1,23]. For simplicity it is assumed in the s-model that ATP, and thus the K(ATP) conductance, is constant, although it is now clear that ATP oscillations occur in β cells [64,66]. The K(ATP) current is $I_{KATP} = g_{KATP}(V - V_K)$. All parameter values for the s-model are given in Table 1.

2.1. Relaxation oscillations

The separation in timescales between the fast variable V and the slow variable s in the s-model gives rise to relaxation oscillations (e.g., [96,101]). Fig. 1A shows the time course of the fast variable, which has the shape of a square wave. The voltage rises slowly during the nadir of the oscillations, which we call the "down phase", and declines slowly during the peak, which we call the "up phase". The transitions between these phases are very rapid. In contrast, the s variable slowly rises during the up phase and slowly declines during the down phase, yielding a sawtooth pattern (Fig. 1B).

The dynamics of relaxation oscillations are best understood in the phase plane (Fig. 2). Here we plot the nullclines, which are
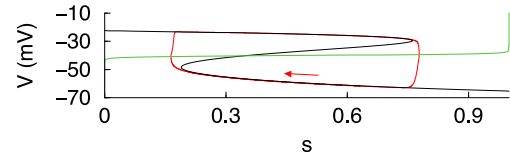

Fig. 2. The trajectory of a relaxation oscillation (red) in the phase plane. Also shown are the V-nullcline (black) and the s-nullcline (green). Here, $v_s = -40$ mV. (For interpretation of the references to color in this figure legend, the reader is referred to the web version of this article.)

the curves where $dV/dt = 0$ and $ds/dt = 0$, respectively, with the trajectory of the relaxation oscillation superimposed. From (3), we see that the voltage nullcline is the curve in which the ionic currents sum to zero. Since this is nonlinear in V, but linear in s, we can specify the V-nullcline by solving for s in terms of V:

$$s = \frac{-(I_{Ca} + I_{Kdr} + I_L + I_{KATP})}{g_s(V - V_K)} \quad . \tag{8}$$

The equation for the s-nullcline is just

$$s = s_\infty(V) = \frac{1}{1 + e^{\frac{v_s - V}{s_s}}} \quad . \tag{9}$$

The nullclines partition the (s, V)-plane into regions of uniform flow direction; the direction of flow switches between left and right when the s-nullcline is crossed and between up and down when the V-nullcline is crossed.

Note that the V-nullcline corresponds to the surface $\{F(\vec{x}, \vec{y}) = 0\}$ in the notation of the general fast subsystem given by Eq. (1). This surface is also known as the *critical manifold*, since it is the surface of critical points of the fast subsystem and has manifold structure; this terminology will be useful later. The critical manifold is Z-shaped, consisting of three branches, pairs of which meet at folds or "knees", which are saddle-node bifurcations of the fast subsystem Eq. (3) for the s-model. The s-nullcline is a sharp sigmoid curve. These cross on the middle branch of the V-nullcline, resulting in an equilibrium point of the full system at which the derivatives of both variables are 0. However, this is an unstable equilibrium, and it is surrounded by a stable limit cycle that is the relaxation oscillation.

Because of the separation of timescales, a typical phase point moves quickly in the V direction to the V-nullcline, governed by the fast subsystem. It then moves slowly along this nullcline as s slowly changes, governed by the slow subsystem. During the down phase of the relaxation oscillation the phase point moves leftward along the bottom branch of the V-nullcline until the branch turns around at the left knee. It then moves rapidly upward to the top branch, again reflecting the fast subsystem dynamics. Now in the up phase, the phase point moves slowly rightward along the top branch of the V-nullcline, driven by the slow subsystem, until the nullcline turns at the right knee. From here the phase point moves rapidly down to the bottom branch of the V-nullcline, and the cycle is restarted.

2.2. Canards

Canards, named in part after the French word for ducks, were first discovered and studied in planar systems yielding relaxation oscillations [6,35,58], mostly the van der Pol oscillator. Canard oscillations occur in a small range of parameter values near an (Andronov)-Hopf bifurcation induced by variation of a single parameter in a fast-slow system. In the case of a planar fast-slow system, they are transitional phenomena that appear at the interface between a stable stationary state and large-amplitude relaxation oscillations. Because the transition from stationarity or small-amplitude oscillations to large-amplitude oscillations corresponds
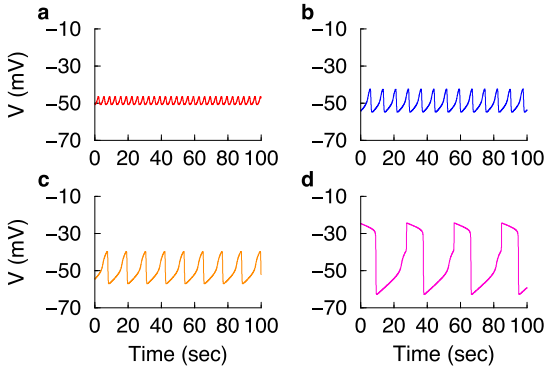
Fig. 3. Time courses of several canards during a canard explosion. **(A)** $v_s = -47.2$ mV. **(B)** $v_s = -46.8604$ mV. **(C)** $v_s = -46.86031215575$ mV. **(D)** $v_s = -46.86031215573$ mV.
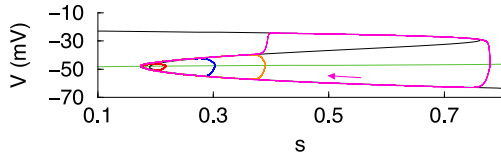

Fig. 4. Trajectories of the four canards from Fig. 3, with the same color correspondence. The s-nullcline shown is for $v_s = -47.2$ mV.

to an exponentially small interval of parameter values, the phenomenon is known as a *canard explosion* [13,58].

Fig. 3 shows several examples of canards in the transition from a stable hyperpolarized equilibrium to a full-blown relaxation oscillation for the s-model. These all occur in the parameter range from $v_s = -47.2$ to -46.86031215573 mV. The first oscillations, shown in panel A, occur very close to a supercritical Hopf bifurcation and have small amplitude with sawtooth shape. As v_s is increased, moving further past the Hopf bifurcation, the oscillations grow and become slower. Panel D shows an example in which the canard oscillation has transitioned into a large-amplitude relaxation oscillation, but with a noticeable shoulder. The changes in shape of the oscillation that occur in the figure are generic in the vicinity of a singular Hopf bifurcation that gives rise to relaxation oscillations [2,3].

An explanation for this canard explosion is again based on a phase plane analysis (Fig. 4). Here, the V and s-nullclines are again shown, but now v_s has been adjusted so that the intersection occurs very close to the left knee, just above the v_s value at which the Hopf bifurcation occurs. Superimposed are the four canard trajectories from Fig. 3. In each case, the trajectory moves along the bottom branch of the V-nullcline, and then it moves some distance up the middle branch before either jumping back to the lower branch (the three smaller orbits) or jumping away to the upper branch (magenta orbit). Indeed, the motion along the middle branch is a hallmark of a canard orbit. The different canards shown here were obtained using different values of the parameter v_s; the canard amplitude increased when v_s was made slightly larger, which translates the s-nullcline upward (the four different s-nullclines are almost indistinguishable, and we show only one of them). The two canards in Fig. 3C and D were obtained with v_s values that differ only at the eleventh decimal place, and between these additional canards exist. Indeed, the "maximal canard", which occurs at v_s values between these two, travels all the way up the middle branch of the V-nullcline before jumping back to the bottom branch. It is possible that the name "canard" also was chosen to label these oscillations because of the word's connotation as French slang for hoax, corresponding to the superficially unbelievable observation that such small parameter changes could yield such significantly different orbits.

Table 2
Parameters for the 3-dimensional s-model (3), (4), (10), based on [91].

$g_{Ca} = 280$ pS	$g_L = 25$ pS	$g_{Kdr} = 1300$ pS
$g_s = 20$ pS	$g_{KATP} = 13$ pS	$C_m = 4524$ fF
$V_K = -80$ mV	$V_{Ca} = 100$ mV	$V_L = -40$ mV
$v_m = -22$ mV	$v_n = -9$ mV	$v_s = -40$ mV
$s_m = 7.5$ mV	$s_n = 10$ mV	$s_s = 0.5$ mV
$\bar{\tau}_n = 8$ msec		

Although canards were first discovered and analyzed in planar fast-slow systems, they are rarely seen in that setting because of the small region of parameter space in which they exist. While interesting and important mathematically, they are of little importance in biological or chemical systems. However, in systems with two or more slow variables, the behavior can be generic, and therefore the importance of canards in such systems is greater. We discuss these later, but first we consider another type of behavior that can be produced in systems with a single slow variable, as long as there are at least three variables in the model in total.

3. Bursting oscillations in systems of dimension ≥ 3

For fast-slow models of 3 or more dimensions, relaxation oscillations can occur that are similar to those in the planar case. In this case, however, the possibility of richer fast and slow subsystem dynamics arises as well. The extensions of the ideas explaining relaxation oscillations in planar fast-slow systems can be used to understand a wide range of bursting dynamics. One complication in bursting is that with fast variables $\vec{x} \in \mathbb{R}^m$ for $m \geq 2$, a fast subsystem attractor may not be a set where $F(\vec{x}, \vec{y}) = 0$. This issue is critical for many forms of bursting activity, but it necessitates the use of some additional mathematical tools in fast-slow analysis.

3.1. Bursting with the s-model

Bursting consists of episodes of fast oscillations, often called spikes, separated by epochs of quiescence. The spiking phase is called the *active phase* and the quiescent phase is called the *silent phase*. To illustrate bursting, we modify the s-model used in the last section by removing the quasi-equilibrium approximation for the delayed rectifier activation variable n. Then, the delayed rectifier K$^+$ current becomes $I_{Kdr} = g_{Kdr}n(V - V_K)$, where the n dynamics are described by

$$\frac{dn}{dt} = \frac{n_\infty(V) - n}{\tau_n(V)} . \tag{10}$$

The time constant function for n is given by

$$\tau_n(V) = \frac{\bar{\tau}_n}{1 + e^{\frac{V - v_n}{s_n}}} . \tag{11}$$

The s-model then consists of the three differential Eqs. (3), (4), (10), and since n is no longer at quasi-equilibrium, the system produces spikes, due to the fast (instantaneous) activation of the Ca^{2+} current and the slower activation of the delayed rectifying current. Parameter values are given in Table 2.

Fig. 5 illustrates an example of bursting produced by this s-model. During part of each cycle, the V and n variables change on a timescale that is much faster than the timescale for s. Indeed, s slowly rises during a burst active phase in response to the voltage spikes (during which the mean voltage is elevated) and slowly declines during a silent phase when the voltage is low. The obvious separation of timescales allows us to bypass a formal dimensional analysis that is helpful in some other systems. In this case, it is clear that V and n can be categorized as fast variables and s as a slow variable.

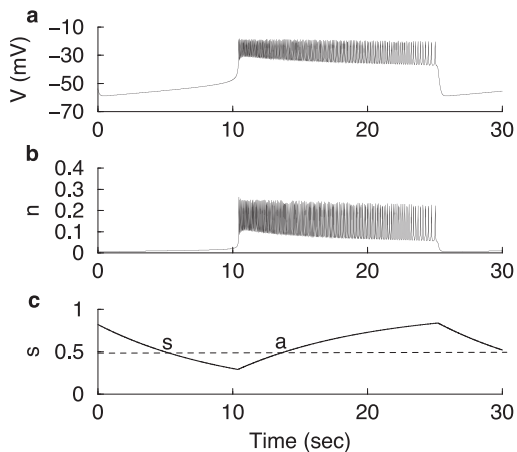**Fig. 5.** **(A)** Bursting oscillations consist of periodic cycles of active and silent phases. An active phase, such as the one shown here, consists of a succession of rapid impulses or spikes; here these are difficult to discern until the end of the active phase because they occur so quickly. **(B)** The activation variable for the delayed rectifier K^+ current responds rapidly to changes in V. **(C)** The activation variable for a second, slowly-activating K^+ current responds slowly to changes in V. For the same value of s (e.g., $s = 0.5$, dashed line), the system can be in either the active "a" or the silent "s" phase.
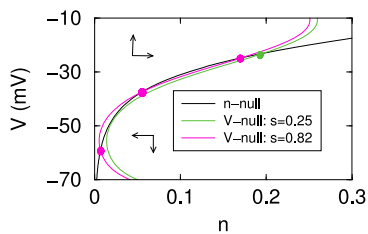

Fig. 6. The nullclines of the fast subsystem, for values of s at the peak and nadir of the s oscillation during bursting. Fast-subsystem equilibria, located at the intersections of the nullclines, are indicated with colored circles.

3.2. Analysis of the fast subsystem

Although it involves only a single timescale, the dynamics of the planar fast subsystem (3) and (10) can best be understood using phase plane analysis, just as with the analysis of the relaxation oscillator. The voltage nullcline is nonlinear in V, but linear in n, so we solve for n in terms of V:

$$n = \frac{-(I_{Ca} + I_s + I_L + I_{KATP})}{g_K(V - V_K)} \quad . \tag{12}$$

The equation for the n-nullcline is also linear in n and nonlinear in V and is given by:

$$n = n_\infty(V) \quad . \tag{13}$$

Example nullclines are plotted in Fig. 6. Importantly, from Eq. (12), it follows that the V-nullcline depends on the slow variable s, which is treated as a parameter of the fast subsystem. During bursting, s ranges from 0.25 to 0.82 (Fig. 5C), so we plot the V-nullcline at these two extreme values of s. It is evident that the nullcline moves leftward when s is increased. Although the change in the nullcline does not seem very great, it results in a change in the equilibrium structure of the system. With $s = 0.25$, the nadir of the s oscillation in Fig. 5, there is a single intersection of the nullclines, and thus a single fast-subsystem equilibrium. With $s = 0.82$, the peak of the s oscillation during bursting, there are three intersections and thus three fast-subsystem equilibria. The two additional equilibria come about via a *saddle-node bifurcation* of the fast subsystem at a point of tangency of the V- and n-nullclines at
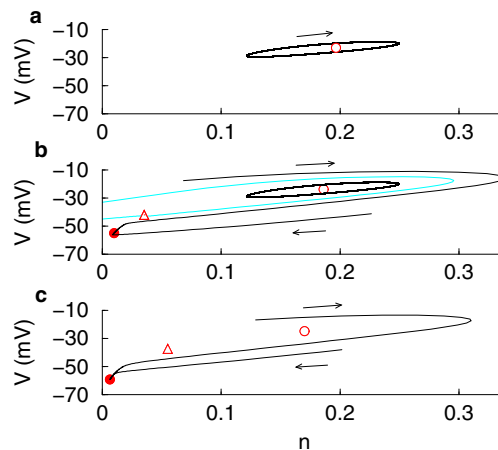

Fig. 7. Phase portraits of the fast subsystem showing equilibria (filled = stable, triangle = saddle point), limit cycles (closed trajectories), some trajectories, and a separatrix (cyan curve connecting to the saddle point). **(A)** $s = 0.25$, **(B)** $s = 0.5$, **(C)** $s = 0.82$. (For interpretation of the references to color in this figure legend, the reader is referred to the web version of this article.)

$s \approx 0.33$, and as s increases, this bifurcation produces equilibria at lower voltages than that of the original equilibrium.

More details about the fast subsystem dynamics are presented in Fig. 7 for three different values of s. When $s = 0.25$ (panel a), corresponding to its nadir during a burst, the single equilibrium is unstable and is surrounded by a stable limit cycle. This reflects continuous spiking that occurs when s is held frozen at this low value. When $s = 0.82$ (panel c), corresponding to its peak during a burst, the high-voltage unstable equilibrium persists, but the limit cycle is now gone. There are now a low-voltage globally stable equilibrium and an intermediate-voltage saddle point. Thus, if $s = 0.82$, the fast subsystem will converge to a steady state at a low voltage. At a value of s between these two extremes, $s = 0.5$, the system has two stable structures: a stable limit cycle reflecting continuous spiking and a stable equilibrium reflecting quiescence at a low-voltage or hyperpolarized state (panel b). The curve that separates the basins of attraction of the two stable structures, called the *separatrix*, is provided by the *stable manifold* of the saddle point (cyan curve), which is locally tangent to the saddle point's stable eigenvector. The basin of attraction of the limit cycle lies inside this separatrix, while the basin of attraction of the stable equilibrium lies outside the separatrix.

Bursting can be understood in terms of the interplay between the fast subsystem phase plane and the slow subsystem dynamics. At the beginning of the active phase, the slow variable s is small, so there is a single stable structure, a limit cycle, in the fast subsystem (as in Fig. 7A). The resulting sustained spiking of (V, n) increases the mean value of V, which in turn causes s to increase, governed by the slow subsystem Eq. (4). For a range of s values, the system is bistable (as in Fig. 7B), but the system keeps spiking since the trajectory is in the basin of attraction of the limit cycle for each s. As s continues to increase, the limit cycle expands, and it is eventually annihilated through a fast subsystem homoclinic bifurcation at a critical value of s for which the limit cycle connects with the saddle point. For s above this value, the trajectory is attracted to the only attractor of the fast subsystem, namely the stable equilibrium. Once it reaches a neighborhood of this attractor, the slow subsystem dynamics takes over as in the relaxation oscillation case and the silent phase begins. Since V is now hyperpolarized, the slow subsystem dynamics causes s to decline, taking the fast subsystem back through the interval of bistability (as in Fig. 7B). Unlike during the active phase, however, the trajectory is
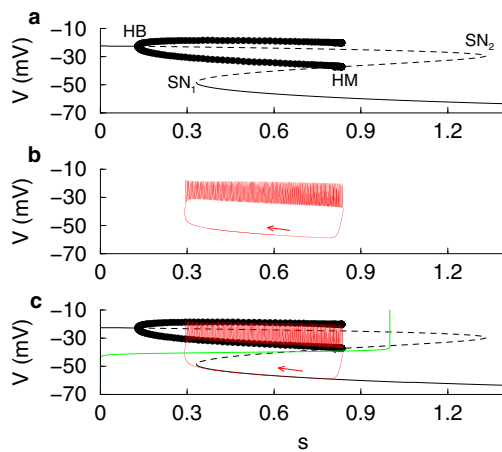
Fig. 8. Fast-slow analysis of bursting. **(A)** A bifurcation diagram of the fast subsystem with s treated as a bifurcation parameter. Solid curves represent stable stationary solutions, while dashed curves represent unstable stationary solutions. The two thick curves represent the minimum and maximum values of V for the periodic branch. HB = supercritical Hopf bifurcation, SN = saddle-node bifurcation, HM = homoclinic bifurcation. **(B)** The bursting trajectory projected into the $s - V$ plane. **(C)** Superposition of the fast subsystem bifurcation diagram (black), the s-nullcline (green), and the bursting trajectory (red). (For interpretation of the references to color in this figure legend, the reader is referred to the web version of this article.)

now in the basin of attraction of the equilibrium, so the trajectory remains at a hyperpolarized voltage. Eventually, as s continues to fall, the stable node and the saddle point coalesce at the fast subsystem saddle-node bifurcation, and the trajectory is now attracted to the stable limit cycle (as in Fig. 7A), restarting the active phase. The fact that the fast subsystem can be either spiking or silent for the same values of s, due to fast-subsystem bistability, is reflected in the bursting shown in Fig. 5; during the rising phase of s the system is spiking, while during the falling phase it is silent.

3.3. Bursting viewed through bifurcation analysis

The fast subsystem analysis can be summarized with a bifurcation diagram, in which s is used as a bifurcation parameter, as illustrated in the projection to the (s, V) plane shown in Fig. 8A. For s near 0 there is a branch of stable equilibria at elevated voltages. A supercritical Hopf bifurcation (HB) occurs near $s = 0.15$; there, the equilibrium branch is destabilized and a branch of stable periodic spiking solutions emerges. The unstable equilibrium branch continues past $s = 1.2$ (the s equilibrium function ranges from 0 to 1, but when treating s as a parameter we are free to make it as small or large as desired) and turns back to the left at a saddle-node bifurcation (SN$_2$). This is not the same as the saddle-node bifurcation discussed earlier, since it involves the coalescence of the high-voltage branch of unstable equilibria with a middle branch of saddle points. The middle equilibrium branch spans an interval of s-values from SN$_2$ down to where it meets the low-voltage equilibrium branch at another saddle-node bifurcation, SN$_1$, which is the bifurcation discussed earlier. The lower equilibrium branch is stable for all values of s for which it exists. Together, these fast subsystem equilibrium branches form a Z-shaped curve, or Z-curve; recall that this is also called the *critical manifold*. Turning now to the periodic solutions, the periodic branch emanating from the HB opens to the right, and both the minimum and maximum voltage values of the oscillation are shown. This family of periodic orbits continues until its termination at a homoclinic bifurcation (HM), where the lower branch of the periodic curve connects with the middle branch of the stationary curve. A key feature of this bifur-

cation diagram is the interval of bistability that extends from SN$_1$ to HM.

The middle panel of Fig. 8 shows the burst trajectory of the full system projected into the (s, V)-plane. Since the bursting is periodic the trajectory is a closed curve, and the spiking at the top of the trajectory reflects the oscillations on the fast timescale. When this trajectory is superimposed onto the fast subsystem bifurcation diagram (Fig. 8C), along with the s-nullcline, the basis of the multiscale oscillation can be deduced. During the active phase the system follows the periodic branch of the Z-curve to the right, on the slow timescale, until the branch ends at the HM bifurcation. From here the trajectory moves down almost vertically, reflecting the fast subsystem dynamics. The trajectory is now attracted to the bottom stationary branch, within a neighborhood of which the slow subsystem dynamics takes over. Since the trajectory has crossed the s-nullcline, the slow motion is now leftward. This drift continues until the bottom equilibrium branch ends at the SN$_1$ bifurcation, after which the trajectory moves almost vertically upward to the periodic spiking branch, governed by the fast subsystem, which restarts the cycle. An important note is that during the active phase, the fast subsystem attractor is the family of stable periodic orbits. These orbits do not satisfy $dV/dt = dn/dt = 0$, and hence, according to what we have introduced so far, the slow subsystem is not well-defined. Mathematically, this issue is handled by *averaging*, such that not V itself, but rather its average over a periodic orbit, appears in the s-equation in the slow subsystem. We refer the reader to [4,16,38,81,94], for example, for details.

What do we learn from this fast-slow analysis of bursting? There are actually several important observations that can be made that would not be so easily deduced without such an analysis. First, since the branch of fast subsystem periodic orbits terminates at a homoclinic bifurcation, where period approaches infinity, we expect the spike frequency to decline near the end of the active phase of bursting. Although not evident from the voltage time course shown in Fig. 5A, this is in fact what happens. Another observation that comes from the fast-slow analysis is that it should be possible to reset the bursting from active to silent, or silent to active, with a brief perturbation. This is because the fast subsystem is bistable, so an appropriate perturbation can move the system from one basin of attraction to the other. Furthermore, if the system is reset from silent to active phase, then the resulting active phase should be shorter than its normal duration (and similarly for an active-to-silent reset, resulting in a short silent phase).

While these observations involve the structure of the fast subsystem bifurcation diagram, other observations involve the s-nullcline as well. Any intersection of this nullcline with an equilibrium branch of the fast subsystem is an equilibrium of the full system. If the intersection occurs on the lower branch of the Z-curve, then the equilibrium will be stable, so the full system will not burst but will instead be at a hyperpolarized equilibrium. If the intersection occurs on the stable portion of the upper branch of the Z-curve, then the equilibrium will again be stable, but now the system will be at a depolarized equilibrium. This is referred to as *depolarization block* and is typical of many excitable systems with excessive stimulatory input. If the intersection occurs on the middle branch between SN$_1$ and HM, as in Fig. 8C, then the full-system equilibrium is unstable and bursting will occur. Finally, if the nullcline intersects the Z-curve middle branch above the HM, cutting through the periodic branch, then in the limit $\tau_s \to \infty$, the full system will spike continuously. Away from this limit the system may either spike continuously or burst, depending on the value of τ_s and on how close the intersection is to the HM [7]. The s-nullcline can be adjusted by changing either v_s or s_s; increasing v_s translates the nullcline upward, while increasing s_s changes the slope of the nullcline so that it is less like a step function.

Adjusting either parameter can convert bursting to continuous spiking or to a steady state.

3.4. Phantom bursting: The advantage of two slow variables

The bursting described thus far relies on two things: bistability in the fast subsystem and the appropriate intersection of the slow nullcline with the Z-curve. Both of these restrictions, which limit the region of parameter space for which bursting occurs, arise due to the fact that there is a single slow variable. If a second slow variable is introduced into the system, both restrictions are removed and bursting can become more robust. This effect was first demonstrated in the case of bursting in neuron R15 of *Aplysia* [63]. The bursting produced here has low spike frequency at both the beginning and the end of the active phase, so the frequency profile is shaped like a parabola. Rinzel explained this *parabolic bursting* using fast-slow analysis [83] with a published model, the Plant model, that contained two slow variables [76]; it can also occur with a simpler phase model, with just one fast variable that evolves on a circle, as long as two slow variables are present [4]. If one constructs a fast subsystem bifurcation diagram using one of the slow variables, say s_1, as a bifurcation parameter, then there is no region of bistability. Instead, the periodic branch terminates at the SN_1 bifurcation, in what is known as a *Saddle Node on Invariant Circle* (or SNIC) bifurcation, making it impossible for bursting to occur if there were only a single slow variable. However, if, as in the Plant model, there is a second slow variable s_2 that slowly shifts the fast subsystem bifurcation back and forth as it varies, then bursting is possible. Indeed, there are fast subsystem SNIC bifurcations along a whole curve in (s_1, s_2)-parameter space. Furthermore, since the bursting trajectory now intersects this curve, and hence passes near a fast subsystem homoclinic orbit, at both the beginning and the end of the active phase, the bursting will be parabolic.

We focus now on a more recent example, in which fast-subsystem bistability is present, but the slow nullcline intersects the Z-curve in a way such that bursting would not occur if there were not a second slow variable [8]. We use the 4-dimensional system that we refer to as the "phantom bursting model":

$$\frac{dV}{dt} = -(I_{Ca} + I_{Kdr} + I_{Ks1} + I_{Ks2} + I_L)/C_m \tag{14}$$

$$\frac{dn}{dt} = \frac{n_\infty(V) - n}{\tau_n(V)} \tag{15}$$

$$\frac{ds_1}{dt} = \frac{s_{1\infty(V)} - s_1}{\tau_{s1}} \tag{16}$$

$$\frac{ds_2}{dt} = \frac{s_{2\infty(V)} - s_2}{\tau_{s2}} \; . \tag{17}$$

This system is very similar to the s-model, but there are some changes. The slow variable s has been renamed s_1 and the time constant τ_{s1} reduced to make it faster. Also, the slope parameter s_{s1} has been increased from 0.5 mV (see Table 1) to 10 mV. A second slow variable s_2 has been introduced with a time constant that is much greater than τ_{s1}. This is the activation variable for a K⁺ current, called I_{s2}, that replaces the constant-conductance K⁺ current (I_{KATP}) used in the s-model. Parameter values are shown in Table 3.

Fig. 9A shows the bursting produced by this model. When the second slow variable, s_2, is clamped at its average value at t=50 s the bursting abruptly terminates and the system becomes silent. Had s_2 been clamped during the burst active phase then the system would have entered a continuous spiking state instead. In either case, bursting is prohibited when s_2 is not allowed to oscillate. This lack of bursting arises in spite of the fact that the oscillations
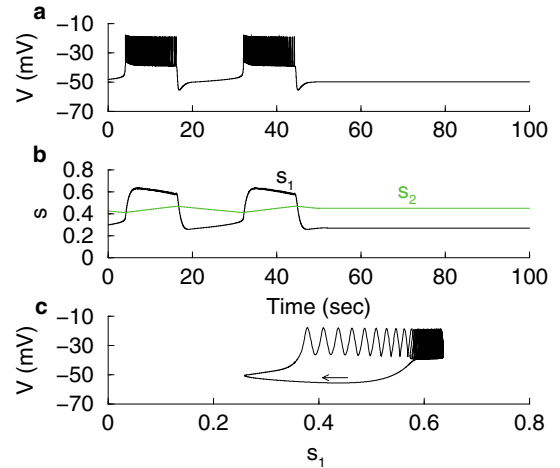
Fig. 9. Bursting produced by the model with two fast and two slow variables. **(A)** Bursting is terminated when the second slow variable is clamped at its mean value ($s_2 = 0.45$) at time t = 50 s. **(B)** The oscillation profiles of the two slow variables are quite different, due to their different time constants. Variable s_1 changes more rapidly than does s_2. **(C)** Projection of the burst trajectory in the $s_1 - V$ plane.
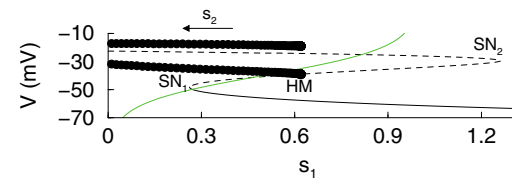

Fig. 10. The fast subsystem bifurcation diagram and superimposed slow s_1 nullcline for the model with two fast and two slow variables. In this diagram $s_2 = 0.45$, but when s_2 is allowed to vary it shifts the fast subsystem bifurcation diagram leftward as it increases, as indicated with the arrow.

in s_2 are rather small, as shown in Fig. 9B. In fact, the s_1 oscillations are much larger, since s_1 changes much faster than s_2.

Using the fast-slow perspective that was presented for the s-model, we view the burst trajectory by projecting it into the $s_1 - V$ plane (Fig. 9C). Although there are similarities to the burst trajectory with the s-model, there are also major differences. Most significantly, s_1 does not increase monotonically during the active phase, but instead the trajectory turns around near the end of the active phase as s_1 declines, causing an overlap in the projection. This can be understood by again looking at the fast subsystem bifurcation diagram (Fig. 10), which is actually a snapshot at $s_2 = 0.45$, with the superimposed s_1 nullcline. Because the nullcline is less steep than in the s-model, it now crosses the Z-curve at several locations. Most importantly, it intersects the bottom branch of stable equilibria and the periodic branch of stable spiking solutions. Thus, when s_2 is clamped, the full system will be bistable, with a stable hyperpolarized equilibrium and a stable continuous spiking solution, explaining what we observe in Fig. 9A when s_2 is clamped.

When s_2 is allowed to vary, however, its increases move the fast subsystem bifurcation diagram to the left and its de-

creases move the diagram to the right. Thus, during a silent phase when the trajectory is following the lower branch of the Z-curve, it reaches the point of intersection with the nullcline, where $ds_1/dt = dV/dt = dn/dt = 0$, and must wait for s_2 to decline sufficiently so that SN_1 passes the nullcline before escaping and making a fast jump to the active phase. After this transition, the trajectory moves rightward along the periodic branch until it converges to the continuous spiking state corresponding to the intersection of the s_1-nullcline with the family of periodic orbits. Then it must wait for s_2 to increase sufficiently so that the HM bifurcation moves past the intersection. Since the periodic branch moves along with the Z-curve, and the motion is to the left, the spiking trajectory will drift back leftward during the latter portion of the active phase, resulting in the overlap observed in Fig. 9C.

The bursting scenario described above has been called *phantom bursting* [8]. The name stems from the observation that the burst period can be quite different from the time constants of the two slow variables, so if one wishes to determine the identity of the slow process driving bursting by correlating the burst period to the time constant of any slow variable, the identification will be inconclusive. Indeed, the bursting is driven by a combination of the two slow variables, and the contribution made by each will vary depending on both fast- and slow-subsystem parameters [112]. Importantly, because phantom bursting does not require that the slow nullcline intersect the fast subsystem bifurcation diagram in any restrictive way, the parameter range in which phantom bursting can be generated is much larger than that for bursting driven by a single slow variable.

3.5. What biologists can get from fast-slow analysis

While fast-slow analysis may seem relatively abstract, it can actually be quite useful in understanding biological systems, particularly when analysis of the model is done in conjunction with experimental studies. One example is the study of developing neural networks in the spinal cord, where all synaptic coupling is excitatory. One might expect this network to be very active, given the purely positive interactions among neurons. Instead, the network is mostly silent, with occasional episodes of activity [71]. A modeling study proposed that the network bursting activity is due to synaptic depression, so when the cells spike together the strength of the coupling between them slowly weakens due to depression. A mean field model was designed that could be analyzed in the phase plane, and it exhibited relaxation oscillations. It was then simple to demonstrate that electrical perturbations applied during the silent phase of the network burst could elicit a premature episode of activity, and that the duration of the premature episode should be longer when the stimulus is applied later in the silent phase [98]. This can be understood from Fig. 2. When the trajectory is moving along the bottom branch ("off" phase), if V is perturbed upward across the middle branch, then it will be attracted to the top branch ("on" phase) and move rightward until the upper knee is reached. This is the premature activity episode. This prediction was tested in the laboratory on embryonic spinal cords and shown to be valid. In addition to this prediction, the model predicted that, in the presence of noise, there should be a positive correlation between the duration of the preceding inter-episode duration and the episode duration, but not between the episode duration and the following inter-episode duration. This model prediction was also validated experimentally [98]. So this example illustrates how the development of a simple model and fast-slow analysis of the model can be important in interpreting experimental data and in designing new experiments.

Another example of the utility of fast-slow analysis to biologists involves the effects of glucose on the bursting pattern of pancreatic β-cells. At a low glucose concentration, the β-cells are typically silent. At higher glucose levels they begin to burst, and as the glucose level is increased the duty cycle (active phase duration divided by the total oscillation period) increases [70], increasing the amount of insulin secreted. The very first model for β-cell electrical activity was able to account for this, assuming that the ATP generated by metabolism of internalized glucose increases the activity of Ca^{2+} pumps in the plasma membrane of the cell [22]. The extra pumping activity slows down the accumulation of Ca^{2+} that occurs during a burst active phase, and speeds up the removal of intracellular Ca^{2+} during the silent phase. Thus, at higher glucose levels the active phases get longer and the silent phases get shorter, increasing the duty cycle. This was later elegantly explained using fast-slow analysis of the model [78] and the explanation can be understood from Fig. 8. The glucose can be thought of as translating the s-nullcline upward in this figure. With low glucose it intersects the bottom branch of the Z-curve, so that the system has a stable low-voltage equilibrium. As glucose is increased the intersection rises until it occurs on the middle branch of the Z-curve. In this case the equilibrium is unstable and bursting commences. The speed at which the trajectory travels along the lower branch of the Z-curve depends on the horizontal distance of the trajectory from the s-nullcline; shorter distances typically mean that the trajectory travels more slowly. When the nullcline and Z-curve intersect near the lower knee the trajectory typically travels slowly along the lower branch (long silent phase) and more rapidly along the spiking branch (short active phase), yielding a low duty cycle. At higher glucose, the nullcline is translated upward so that the trajectory travels more rapidly along the lower branch (shorter silent phase) and more slowly along the top branch (longer active phase), so that the duty cycle is greater. With sufficiently high levels of glucose the nullcline intersects the spiking branch and the model cell spikes continuously, just as the β-cell does.

4. Robust canard phenomena in non-planar systems

We have seen that in planar fast-slow systems, the switch from quiescent, steady-state behavior to relaxation oscillations via a Hopf bifurcation involves an abrupt transition, over an exponentially small interval of parameter values, through a family of canard solutions that pass along a structure that is repelling for the fast subsystem. Since three-dimensional fast-slow systems can also exhibit transitions from quiescence to relaxation oscillations via Hopf bifurcations, it is natural to expect a similar phenomenon in this setting. Interestingly, the higher-dimensional phase space introduces additional rotations not present in the planar case, giving rise to novel solution classes called mixed-mode oscillations and torus canards, and also provides a significant increase in robustness of canard-related phenomena.

4.1. Mixed-mode oscillations

We first give a general description of the structures that underlie mixed-mode oscillations and the systems that can be used to study them. We aim to introduce enough notation to be precise and to equip readers to begin to study these phenomena in models of interest, while avoiding technicalities. In the next subsection, we proceed to illustrate these ideas with a particular example system.

To understand the phenomenon of mixed-mode oscillations in a minimal setting, we consider the following three-dimensional system, written in notation motivated by neuroscience models:

$$\dot{v} = F(v, n, h), \tag{18}$$

$$\dot{n} = \epsilon N(v, n), \tag{19}$$

$$\dot{h} = \epsilon H(v, h), \tag{20}$$

where the parameter ϵ is very small, $0 < \epsilon \ll 1$, and we suppress reference to all other parameter values. For system (18)–(20), the fast and slow subsystems are 1- and 2-dimensional, respectively. The critical manifold is given by

$$S = \{(v, n, h) : F(v, n, h) = 0\},$$

which generally is a 2-dimensional surface, parameterized by the slow variables n and h.

To connect with the examples considered in the planar case and with the typical situation for many biological models exhibiting a switch from excitability to relaxation oscillations, let us suppose that S is a cubic 2-dimensional surface consisting of 3 planar sheets, $S = S^- \cup S^0 \cup S^+$, connected pairwise at curves, L^- and L^+. Let us also assume that S can be expressed as a graph of a function $n = n(v, h)$ with $F(v, n(v, h), h) = 0$. We can linearize the fast subsystem at any point $\mathbf{p} \in S$ to determine its stability with respect to the fast dynamics; since the fast subsystem is 1-d, linearization amounts simply to computing $F_v(\mathbf{p})$. Assume that the outer sheets $S^{\pm}$ have $F_v < 0$ and hence consist of stable fast subsystem equilibria, while S^0 has $F_v > 0$ corresponding to instability. This simple stability analysis becomes inconclusive when $F_v = 0$, which is the condition for a fold bifurcation for the fast subsystem that we have already seen in the planar case and that holds along $L^{\pm}$.

To continue to generalize from the planar case, suppose that as a particular system parameter is varied, a critical point $\mathbf{p}^*$ of the full system (18)–(20) moves from S^-, where it is stable, to S^0, where, far enough away from L^-, it is unstable. While $\mathbf{p}^*$ is on the stable sheet S^-, with the structure we have described and some additional standard assumptions to ensure a global return, system (18)–(20) has excitable dynamics with the unstable middle sheet S^0 acting as a threshold: a perturbation large enough to push a trajectory from a neighborhood of $\mathbf{p}^*$ across S_0 towards S^+ will yield a transient excursion in phase space followed by a return to the critical point $\mathbf{p}^*$. But what happens when $\mathbf{p}^*$ crosses through the fold L^- into S^0? In the planar case, a canard explosion occurred, so we can expect something interesting in the dynamics of system (18)–(20) as well. With three variables, however, some additional processing and notation, which we shall introduce shortly, are required to describe the situation.

In what we have presented so far about fast-slow analysis, we would try to understand the flow along the critical manifold S by considering the slow subsystem (19) and (20) with v slaved to (n, h) by the requirement $F = 0$. Unfortunately, as we have seen previously, this slaving can break down at the folds $L^{\pm}$, whereas we are interested in dynamics that extends across the folds. Because n is a function of (v, h) along S, however, we can consider the dynamics of (v, h) on S instead of the dynamics of (n, h), which has the advantage that it does not require switching between different sheets if a trajectory crosses a fold. To take this approach in a way that represents dynamics on S, we first implicitly differentiate $F(v, n, h) = 0$ and continue to use $\dot{x}$ to denote dx/dt to obtain

$$F_v \dot{v} + F_n \dot{n} + F_h \dot{h} = 0. \tag{21}$$

In Eq. (21), $\dot{n}$ and $\dot{h}$ are both $\mathcal{O}(\epsilon)$, due to equations (19) and (20). Thus, in our second step, we introduce a slow time $\tau = \epsilon t$, use x' to denote $dx/d\tau$, and combine (21) with Eq. (20) to write

$$-F_v v' = F_n N + F_h H,$$
$$h' = H. \tag{22}$$

System (22) is singular in the sense that $F_v = 0$ at the folds, corresponding to the possible switch to fast dynamics, which means that there is no derivative term in the v equation there. To allow us to study trajectories that do not necessarily exhibit fast jumps as soon as they approach the folds, we take the third and final step of rescaling time by dividing τ by $-F_v$, which is called *desingularization*. Applying this step to system (22) and reverting

back to $\dot{x}$ to denote differentiation by the resulting time variable, with apologies for the abuse of notation, yields the *desingularized reduced system*

$$\dot{v} = F_n N + F_h H,$$
$$\dot{h} = -F_v H. \tag{23}$$

It is important to note that F_v, which is 0 on the folds $L^{\pm}$, has the opposite sign on the outer sheets $S^{\pm}$ of S from what is has on the middle sheet S^0. We continue to assume, without loss of generality, that $F_v < 0$ on $S^{\pm}$ and $F_v > 0$ on S^0. Then trajectories of (22) and (23) have the same orientation on $S^{\pm}$ but orientations are reversed for (23), relative to (22), on S^0.

System (23) has critical points where

$$F_n N + F_h H = 0, \tag{24}$$

$$F_v H = 0 \tag{25}$$

both hold. If $F_n \neq 0 \neq F_h$, then these conditions can be met two different ways, which we denote as follows:

- (CP) $H = N = 0$, or
- (FS) $F_v = F_n N + F_h H = 0$.

If (CP) holds, then since we are only considering points on S, which is defined by $F = 0$, solutions correspond to critical points of the original full system (18)–(20) as well as of the reduced system (22). If (FS) holds but not (CP), then the fold condition $F_v = 0$ is met, which restricts us to $L^{\pm}$, but we do not have $H = N = 0$ and hence we do not have a true critical point. Points that satisfy (FS) but not (CP) are called ==folded singularities==, while both (FS) and (CP) are satisfied where a true critical point hits a fold $L^{\pm}$.

Now, we can return to considering trajectories that travel along S and reach the fold L^- at a point $x \in L^-$ for parameter values such that $\mathbf{p}^* \in S^0$. If the *normal switching condition*

$$(F_n N + F_h N)|_{x \in L^-} \neq 0$$

is satisfied, then x is called a *jump point* and the trajectory will undergo a fast jump away from L^-. A periodic trajectory that reaches both L^- and L^+ at jump points will be a standard relaxation oscillation. On the other hand, if the normal switching condition fails, then (FS) holds and the trajectory reaches the fold at a folded singularity.

This description leads to (at least) two questions: (1) What type of dynamics results when a trajectory encounters a folded singularity, and (2) How can this scenario be robust in 3 dimensions, where a folded singularity is generically an isolated point on a 1-d fold curve? To address the first question, note that as far as system (23) is concerned, a folded singularity x is a critical point. As such, we can linearize system (23) about x and classify it as a node, saddle, or spiral, just as with any other critical point; we call these points *folded nodes*, *folded saddles*, and *folded spirals*, respectively. Suppose that x is a folded node with real eigenvalues $\lambda_s < \lambda_w < 0$ and corresponding strong and weak eigenvectors v_s and v_w, respectively. There is then a unique trajectory $\gamma_s(t)$ in S^- of (23) that converges to x tangent to v_s. Other than $\gamma_s(t)$, trajectories that asymptotically approach x along S^- do so tangent to v_w. Thus, in the scenario that we have been discussing, if there is a folded node $x \in L^-$, then there exists a *singular funnel* on S^-, bounded on one side by $\gamma_s(t)$ and on the other by the fold itself, which contains a branch of the weak eigenvector v_w. Trajectories that start in the singular funnel are, as the name would suggest, funneled into the folded node.

Under the desingularized reduced flow of (23), trajectories are attracted to a folded node on L^- from regions in both S^- and S^0. But as noted earlier, the flow of the reduced system (22), which represents the original system dynamics, is reversed on S^0 relative

to the flow of (23). Hence, under (22), trajectories approach x from S^- but are repelled from x on S^0. This switch allows trajectories to pass from S^- to S^0 near x for $\epsilon > 0$ sufficiently small; that is, the folded node allows canard dynamics to occur! In light of this observation, $\gamma_s(t)$ is called the *singular strong canard*. Furthermore, it can be shown that in the set-up that we have described, for $0 < \epsilon \ll 1$, the singular funnel perturbs to an open set of initial conditions from which corresponding trajectories pass from a neighborhood of S^- to a neighborhood of S^0 before exhibiting a large amplitude fast excursion away from the fold, as long as the relevant trajectory of (23) meets the fold transversally [14,113]. Given that the linearization of the fast subsystem along the critical manifold sheets S^-, S^0 off of L^- yields nonzero eigenvalues (as we have assumed), these sheets perturb to nearby invariant manifolds [39], say $S^{-,\epsilon}, S^{0,\epsilon}$, for $0 < \epsilon \ll 1$. Interestingly, detailed analysis shows that $S^{-,\epsilon}, S^{0,\epsilon}$ develop rotations near L^-; true canards occur at intersections of $S^{-,\epsilon}, S^{0,\epsilon}$, and they and nearby trajectories not only travel along $S^{0,\epsilon}$ but also inherit small amplitude oscillations in the vicinity of L^- from the rotational structure of $S^{-,\epsilon}$ and $S^{0,\epsilon}$ [113].

Mixed-mode oscillations (MMOs) are solutions consisting of alternating phases of small and large amplitude oscillations. The canard dynamics that we have described can naturally give rise to MMOs, with the small oscillations occurring in the vicinity of the fold, as long as the global dynamics brings trajectories that depart from the funnel back into the funnel. Under additional global conditions, periodic MMOs may occur. Note that the funneling process favors existence and stability of such solutions; as long as there is a global mechanism to return trajectories that depart from x back to the singular funnel in the singular limit dynamics, then they will end up funneled back to x, and stable periodic MMOs will result for $0 < \epsilon \ll 1$ [14]. The funnel structure also provides an answer to question (2), about robustness, as it yields, for fixed parameter values, an entire region of initial conditions that generate canard dynamics, which result in MMOs if the relevant conditions are met; moreover, the folded node together with the funnel represent a structure that naturally persists over significant intervals of parameter values. Finally, as far as the generality of this form of dynamics, it should also be noted that this same scenario applies in systems including more than one fast variable [114]. In that case, the core of the dynamics near the fold is still represented by a 3-dimensional system with one fast and two slow variables.

4.2. Mixed-mode oscillations in the Hodgkin–Huxley equations

Mixed-model oscillations are not typically associated with the classical exploration of firing in the squid giant axon by Hodgkin and Huxley that provided the fundamental mathematical framework in which a whole galaxy of neuronal models have been constructed [47]. Surprisingly, many years after the model's original formulation, a form of mixed-mode oscillations was reported in the Hodgkin–Huxley (HH) equations, with slowed ionic time constants corresponding, for example, to low temperature dynamics [32]. It was subsequently established that these MMOs truly fit the two-slow-variable canard-induced MMO framework, and a more complete characterization of the effects of particular time constants on these solutions was provided [87,88]. While a range of other HH-type neuronal models support MMOs without low-temperature adjustments (see [29], Table 5), we take advantage of the thorough exploration and relative low-dimensionality of the HH equations and use that system to illustrate MMOs here.

Taking a quasi-steady state approximation for the fastest activation variable in the model, which turns out to be a center manifold reduction [87], and nondimensionalizing yield the following three-dimensional HH system:
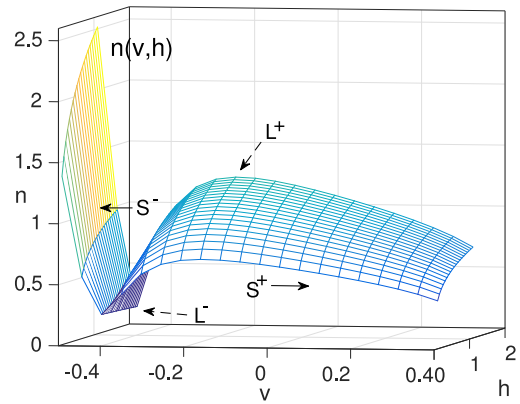

Fig. 11. The surface $\{v' = 0\}$ for the HH system (26) with $I = 9.6$, oriented to emphasize that n can be treated as a function $n(v, h)$ as given by (27). Solid arrows indicate attracting sheets of the surface, $S^{\pm}$, while dashed arrows indicate folds $L^{\pm}$.

$$\epsilon v' = [I - m_\infty^3(v)h(v - E_{Na}) - g_K n^4(v - E_K) - g_L(v - E_L)],$$
$$h' = (h_\infty(v) - h)/(\tau_h t_h(v)),$$
$$n' = (n_\infty(v) - n)/(\tau_n t_n(v)), \qquad (26)$$

where $\epsilon = C_m/120 \ll 1$ for membrane constant C_m, where $\tau_h = \tau_n = 1$ in the classical case (omitting units here and simply assuming that appropriate units have been chosen to render system (26) dimensionless), where the functions in the model are given by

$$\alpha_m(v) = \frac{(100v + 40)/10}{1 - \exp(-(100v + 40)/10)},$$
$$\beta_m(v) = 4\exp(-(100v + 65)/18),$$
$$\alpha_h(v) = 0.07\exp(-(100v + 65)/20),$$
$$\beta_h(v) = 1/(1 + \exp(-(100v + 65)/20)),$$
$$\alpha_n(v) = \frac{(100v + 55)/100}{1 - \exp(-(100v + 55)/10)},$$
$$\beta_n(v) = 0.125\exp(-(100v + 65)/80),$$

with $x_\infty(v) = \alpha_x(v)/(\alpha_x(v) + \beta_x(v))$ for $x \in \{m, h, n\}$, $t_h(v) = 1/(\alpha_h(v) + \beta_h(v)), t_n(v) = 1/(\alpha_n(v) + \beta_n(v))$, and where $g_K = 0.3, g_L = 0.0025, E_{Na} = 0.5, E_K = -0.77, E_L = -0.544$ with I, C_m specified in figure captions below.

The fast subsystem in system (26) consists of the v-equation alone, while the h, n equations form the slow subsystem. MMOs, if they exist, should therefore follow an attracting branch of the critical manifold $\{v' = 0\}$ up to a fold containing a folded node singularity. We can express $v' = 0$ as

$$n = \left[\frac{I - m_\infty^3(v)h(v - E_{Na}) - g_L(v - E_L)}{g_K(v - E_K)}\right]^{1/4}, \qquad (27)$$

which is indeed a cubic-shaped surface with attracting inner and outer branches, a repelling middle branch, and folds joining the repelling branch to each of the attracting ones (Fig. 11). Sure enough, for appropriate choices of $I, \epsilon, \tau_h, \tau_n$, with at least one of $\tau_h, \tau_n >$ 1, a folded node singularity and MMOs exist. The MMOs consist of repeated cycles comprising a slow passage along the low-voltage (hyperpolarized) attracting branch of $\{v' = 0\}$, small-amplitude oscillations in the vicinity of the lower fold near the folded node, a fast jump away from the fold, and then one or more global excursions, composed of a slow passage along the high-voltage attracting branch of $\{v' = 0\}$ and a fast jump back to the low-voltage branch. Each such excursion may land in the funnel of the folded node, completing an MMO cycle, or may miss the funnel, in which case at least one more global excursion is needed; for sustained MMOs to occur, some global excursion must eventually culminate
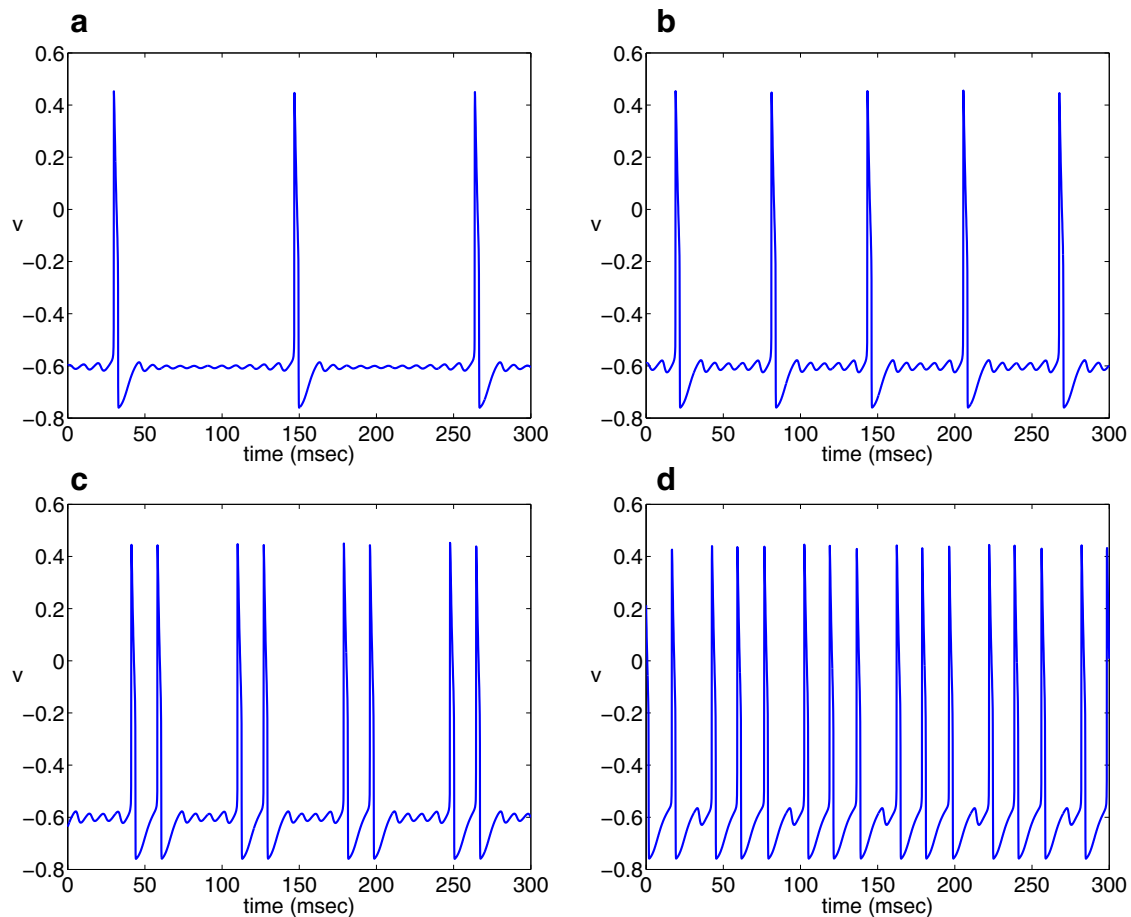
Fig. 12. Time courses of MMOs for the HH Eq. (26) with $\tau_h = 3$, $\tau_n = 1$, $C = 0.84$. MMO patterns for different parameter values include different numbers of small oscillations and global excursions per cycle. **(A)** MMOs for $I = 7.9$ with one global excursion per cycle. **(B)** MMOs for $I = 8.4$ with one global excursion per cycle. **(C)** MMOs for $I = 8.9$ with two global excursions per cycle. **(D)** MMOs for $I = 9.3$ with three global excursions per cycle.

with the entry of the trajectory into the funnel. Time courses of example MMOs appear in Fig. 12. Some involve one global excursion per cycle, others include more. For some of these examples, the small oscillations in the full (v, h, n)-phase space are visualized in Fig. 13.

4.3. Torus canards

As a final example of dynamics arising specifically in multiple-timescale systems, we consider a more complicated form of canards known as *torus canards*. Recall from our presentation of bursting that the bursting solutions considered could be represented as the composition of a silent phase, with slow drift along a lower branch of the critical manifold (Z-curve), a fast jump away from that branch at a fast subsystem fold bifurcation, an active phase combining oscillations on the fast timescale with slow drift on the slow timescale, and a fast jump back to the lower branch at a fast subsystem homoclinic bifurcation where the fast oscillations end. This form of dynamics was enabled in a system with 2 fast variables and 1 slow variable by the fact that the nullcline of the slow variable intersected the Z-curve at an appropriate point on its middle branch. If that intersection point occurred on the lower branch of the Z-curve, on the other hand, then the intersection point was a stable rest or quiescent equilibrium state for the full system, while if the intersection was higher up the branch, then sustained stable, periodic oscillations, corresponding to tonic spiking, could result.

Just as we encountered canards in the transition from lower to middle branch equilibria in a planar system, as well as in the transition of an equilibrium from S^- to S^0 in the non-planar case, we can expect canard solutions in the transition from stable rest to bursting. And also as in those cases, these canard solutions should be characterized by passage near a fold from an attracting to a repelling structure for a fast subsystem, which would arise at parameter values near where the intersection of the slow nullcline and the Z-curve lies at the fold. These would be standard canards, arising on an exponentially small parameter interval, similar to the scenario observed in the planar case; the second fast variable does not qualitatively alter this canard explosion.

Torus canards, on the other hand, may occur, under the right circumstances, at the transition between bursting and tonic spiking. The new feature with torus canards is that the folded structure across which they pass is not a simple fold or saddle-node bifurcation for the fast subsystem, but rather a saddle-node of periodic orbits (SNPO) bifurcation. That is, suppose that the family of fast subsystem periodic orbits in the bursting scenario terminates in an SNPO instead of a homoclinic, as occurs in some biological models [9,15,28,54]. At the SNPO, a stable family of fast subsystem periodic orbits, call it $\mathcal{P}$, comes together with an unstable family, which in turn, in the bursting scenario, terminates in a homoclinic bifurcation on the middle branch of the Z-curve. A bursting trajectory that is following $\mathcal{P}$ will typically jump down to the silent phase from a neighborhood of the SNPO. Near the transition to tonic spiking, however, a canard mechanism may allow the trajectory to travel beyond the SNPO and track the unstable
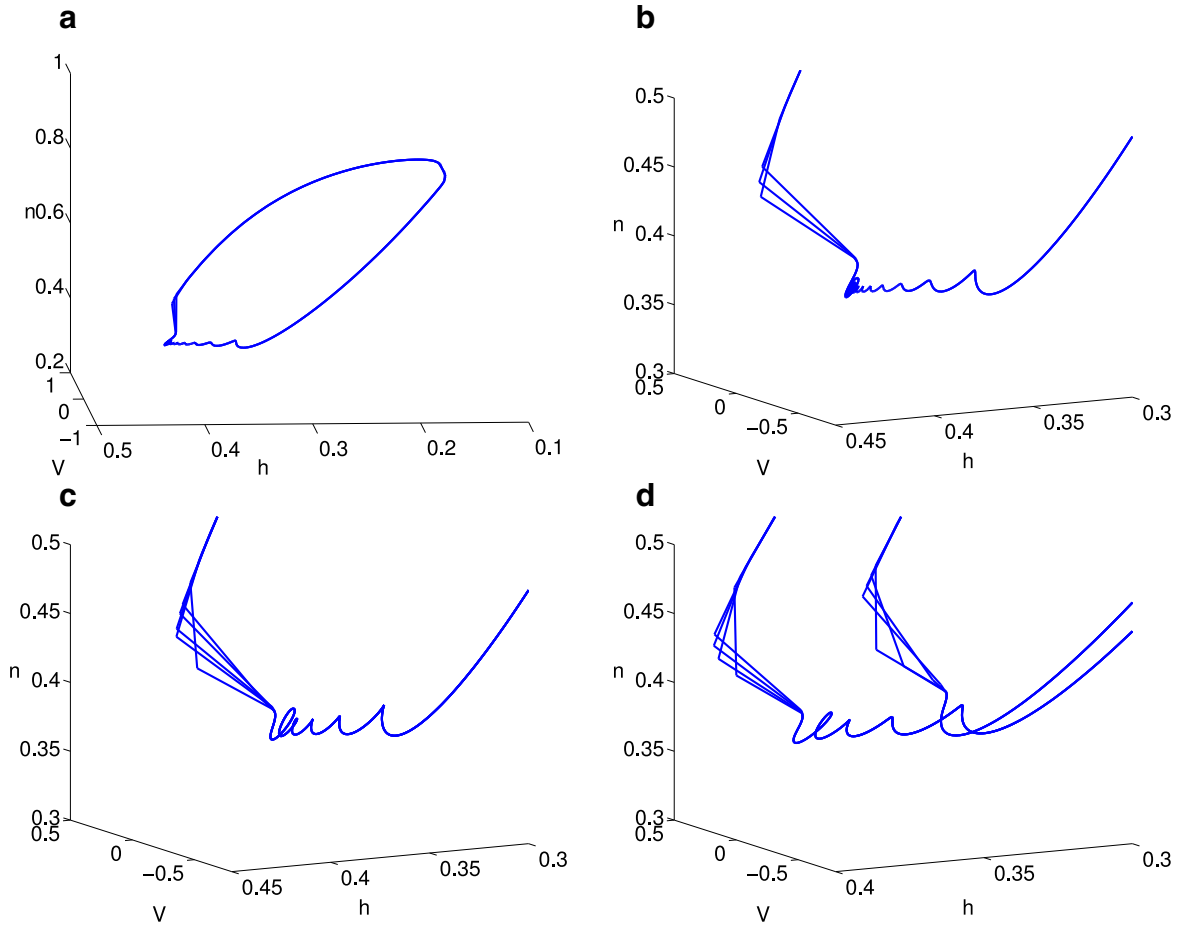
Fig. 13. Phase space views of MMOs for the HH Eq. (26) with $\tau_h = 3$, $\tau_n = 1$, $C = 0.84$. **(A)** Full MMO solution for $I = 7.9$ (cf. Fig. 12A). **(B)** Zoomed view shows trajectories entering the singular funnel (from the right) and engaging in small-amplitude oscillations before exiting the neighborhood of the fold of $\{v' = 0\}$ (to the left) for $I = 7.9$ (cf. Fig. 12A). **(C)** Zoomed view with $I = 8.4$ (cf. Fig. 12B). **(D)** Zoomed view with $I = 8.9$. Note that some trajectories come in from the right and leave again without engaging in any small-amplitude oscillations. These orbits are not in the singular funnel and correspond to the first in a pair of successive global excursions, which occurs between periods of small-amplitude oscillations for this value of I (cf. Fig. 12C).

periodic orbits before jumping down. That is, the passage near the SNPO plays the role of the passage near the fold that occurs with standard canards, while the resulting excursion along the unstable family of periodics is analogous to the excursion along a repelling structure such as S^0 in the standard case.

Although torus canards have been found in some 3-dimensional neuron models [15,28], we present a nice example provided by a 5-dimensional model for a Purkinje cell in the cerebellum (proposed as a reduction of a model with over 6000 variables [54]). We present the model in the form given in [15], namely

$$C\dot{V} = -J - I_L - I_{CaH} - I_{NaF} - I_{KDR} - I_M,$$
$$\dot{m}_i = \alpha_i(1 - m_i) - \beta_i m_i,$$
$$\dot{h}_{NaF} = \alpha_{NaF}(1 - h_{NaF}) - \beta_{NaF}h_{NaF} \qquad (28)$$

for each $i \in \{CaH, KDR, KM\}$. In system (28), V denotes voltage and the terms on the right-hand-side of the voltage equation represent an externally applied current J, a leak current $I_L = g_L(V - V_L)$, a high-threshold non-inactivating calcium current $I_{CaH} = g_{CaH}m_{CaH}^2(V - V_{CaH})$, a fast inactivating sodium current $I_{NaF} = g_{NaF}m_{NaF,\infty}^3 h_{NaF}(V - V_{NaF})$, a delayed rectifier potassium current $I_{KDR} = g_{KDR}m_{KDR}^4(V - V_{KDR})$, and an M-type (muscarinic) potassium current $I_M = g_{KM}m_{KM}(V - V_{KM})$. We follow previous work and treat m_{KM} as the single slow variable in the model [15].

The rate functions take the forms

$$\alpha_{CaH} = 1.6/(1 + e^{-0.0072(V-5.0)}),$$
$$\beta_{CaH} = 0.02(V + 8.9)/(-1 + e^{0.2(V+8.9)}),$$
$$\alpha_{NaF} = \alpha_{n,NaF}/\alpha_{d,NaF}, \quad \alpha_{n,NaF} = 1.0/(1 + e^{(V+59.4)/10.7}),$$
$$\alpha_{d,NaF} = 0.15 + 1.15/(1 + e^{(V+33.5)/15}),$$
$$\beta_{NaF} = (1 - \alpha_{n,NaF})/\alpha_{d,NaF},$$
$$\alpha_{KDR} = \alpha_{n,KDR}/\alpha_{d,KDR}, \quad \alpha_{n,KDR} = 1.0/(1 + e^{-(V+29.5)/10}),$$
$$\alpha_{d,KDR} = 0.25 + 4.35e^{-|V+10.0|/10.0},$$
$$\beta_{KDR} = (1 - \alpha_{n,KDR})/\alpha_{d,KDR},$$
$$\alpha_{KM} = 0.02/(1 + e^{-0.2(V+20.0)}),$$
$$\beta_{KM} = 0.01e^{-(V+43.0)/18.0}. \qquad (29)$$

The function $m_{NaF,\infty}$ is given by

$$m_{NaF,\infty} = 1.0/(1 + e^{-0.1(V+34.5)}),$$

while remaining parameter values are listed in Table 4 [15].

Model (28) and (29) generates tonic spiking for $J = -34.0$ nA and below (Fig. 14A). As noted with our previous discussion of bursting, the tonic spiking solution corresponds to a stable periodic orbit for which the leftward and rightward drift of the slow variable m_{KM} are balanced, which yields pinning to a very small part of the stable periodic orbit family in the fast subsystem bifurcation diagram (Fig. 15A).

Table 4
Parameters for the reduced Purkinje cell model (28) and (29) [91].

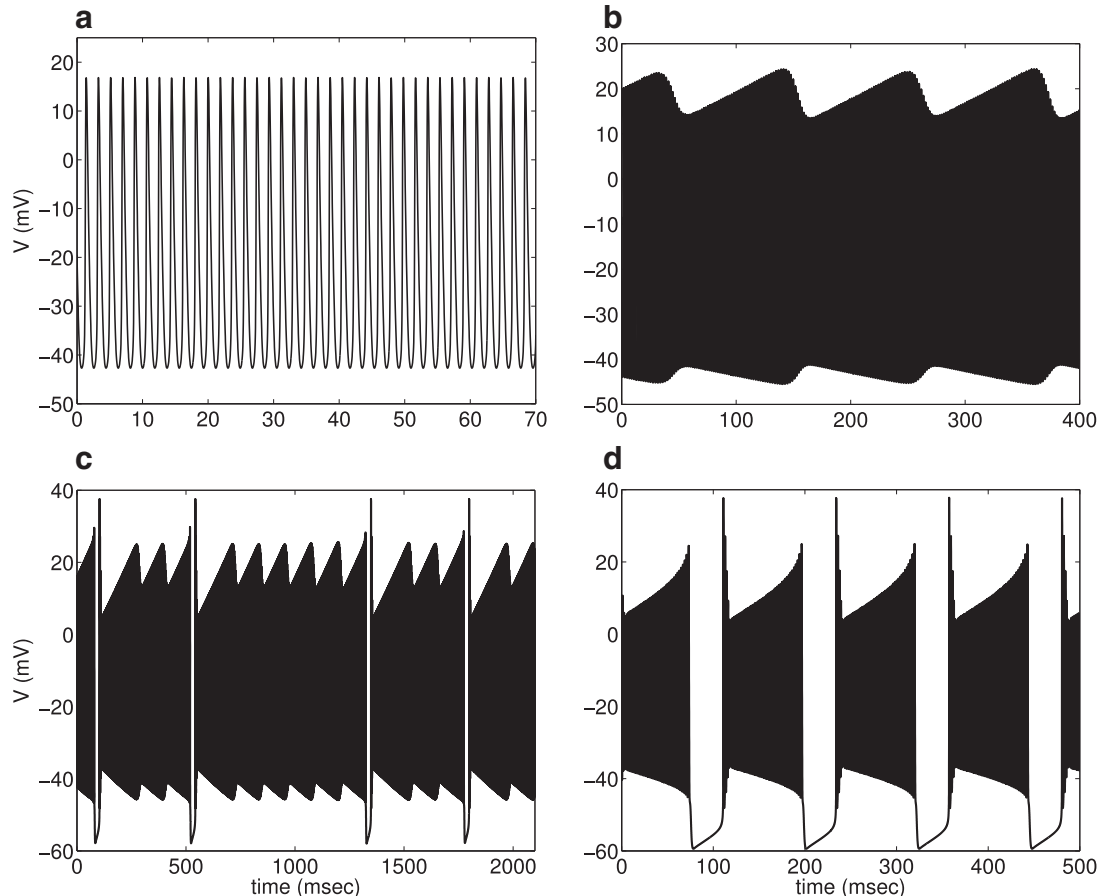| channel	reversal potential (mV)	conductance (μmho)
leak (L)	$V_L = 70$	$g_L = 2$
high-threshold calcium (CaH)	$V_{CaH} = 125$	$g_{CaH} = 1$
fast sodium (NaF)	$V_{NaF} = 50$	$g_{NaF} = 125$
delayed rectifier potassium (KDR)	$V_{KDR} = -95$	$g_{KDR} = 10$
M-current (KM)	$V_{KM} = -95$	$g_{KM} = 0.75$

Fig. 14. Time courses in the transition from spiking through torus canards to bursting for model (28) and (29). Note the different horizontal timescales in different panels. **(A)** Periodic tonic spiking for $J = -34.0$ nA. **(B)** Periodic amplitude-modulated tonic spiking corresponding to a headless torus canard for $J = -32.94$ nA. **(C)** Amplitude-modulated bursting corresponding to a torus canard with a head for $J = -32.93828$ nA. **(D)** Periodic bursting for $J = -30.0$ nA.

As J is increased, for example to -32.94 nA, the model exhibits amplitude-modulated spiking (Fig. 14B). In this regime, there are no silent phases, but a projection of the trajectory onto the fast subsystem bifurcation diagram in (m_{KM}, V)-space suggests that this solution is a torus canard, following a family of stable periodic orbits, crossing an SNPO, and then following a family of unstable periodic orbits before jumping back to the stable periodic branch on each cycle (Fig. 15B). This type of canard solution, with alternation between just two branches of a cubic structure, is sometimes referred to as a *headless canard*, or in this case, a headless torus canard.

Further increases in J yield *torus canards with heads*. These solutions also involve at least one passage from a stable to an unstable branch of fast subsystem periodic orbits, but in this case, a subsequent fast jump carries the trajectories back to a small neighborhood of the lower branch of fast subsystem equilibria on the critical manifold. Thus, each features a true silent phase and qualifies as a bursting solution. Fig. 14C shows a seemingly aperiodic torus canard pattern that features visibly amplitude-modulated spiking within each active phase, corresponding to multiple pas-

sages along each periodic orbit branch before the fast jump to the lower branch. Finding such a solution requires tuning J very precisely; we used $J = -32.93828$ nA, while a similar pattern was shown previously for $J = -32.93825$ nA [54]. For a much broader parameter range, we find periodic torus canards with heads that lack obvious spiking amplitude modulation in the active phase but that still include excursions along the unstable periodic orbit family (Fig. 15C).

Torus canards with heads last up to approximately $J = -31.2$ nA, above which regular bursting, with a jump down at the SNPO, takes over (Figs. 14D,15 D). Of course, more sophisticated methods than direct simulations, starting with bifurcation studies of the full model, would be needed to pinpoint the exact J values where transitions between solution types occur, and still more work would be needed to explain the mathematical details of the dynamic mechanisms involved.

As it stands now, however, mathematical theory that rigorously nails down the properties of torus canards is still far from complete. It appears that in the torus canard scenario, as a bifurcation parameter is varied starting from the tonic spiking regime,
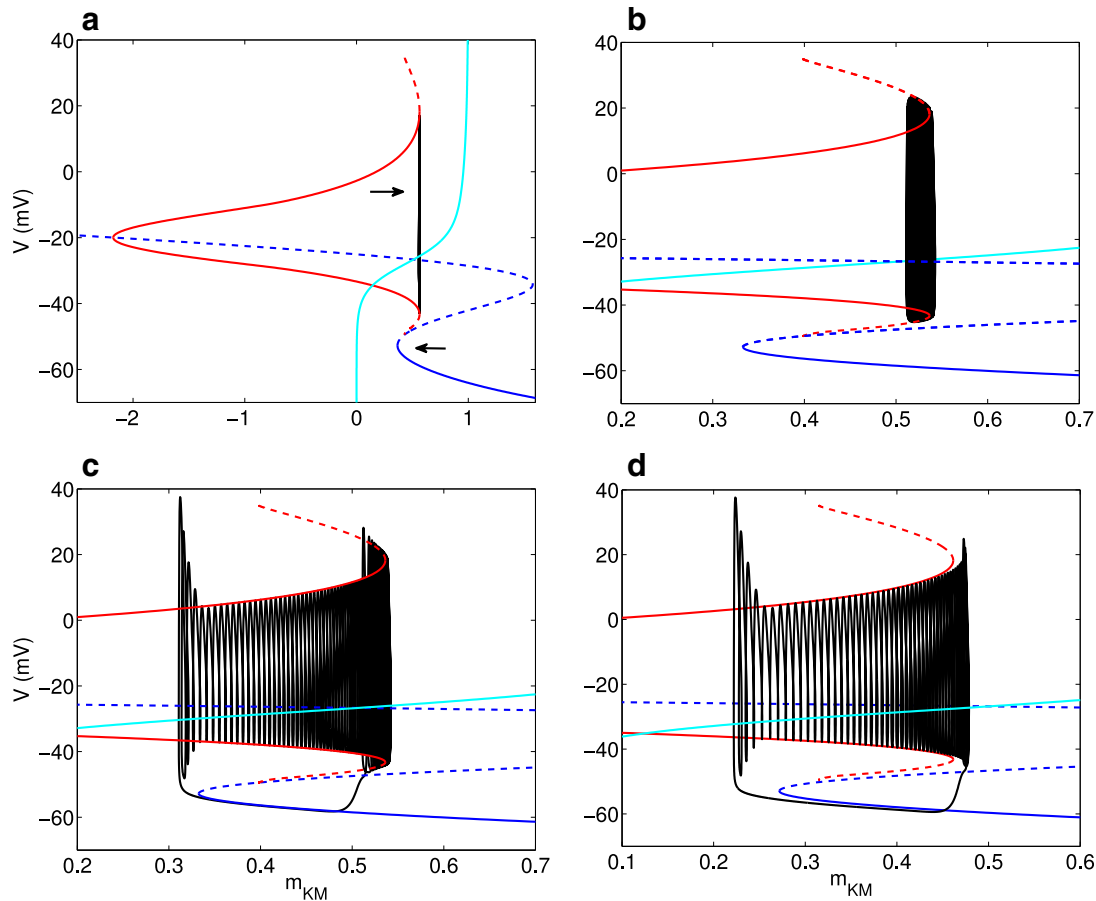
Fig. 15. Projections of solution trajectories onto fast subsystem bifurcation diagrams for model (28) and (29). In all diagrams, the solid (dashed) blue curve is the critical manifold (Z-curve) of stable (unstable) fast subsystem critical points, the solid (dashed) red curves are the maximum and minimum voltages of families of stable (unstable) fast subsystem periodic orbits that meet in a SNPO bifurcation, the black curve is an attracting model trajectory, and the cyan curve is the slow (m_{KM}) nullcline. Note the differences in axis scales across panels; in **(B)**-**(D)**, we have zoomed in, but the same right knee (at large m_{KM}) and Hopf bifurcation (at large negative m_{KM}) structures are present. **(A)** Tonic spiking for $J = -34.0$ nA. Arrows denote direction of change of m_{KM} in each region, which is similar in other panels; spiking trajectory passes above and below the m_{KM}-nullcline. **(B)** Periodic amplitude-modulated tonic spiking corresponding to a headless torus canard for $J = -32.94$ nA. When the trajectory reaches the SNPO, its net drift switches from right to left and it follows the branch of unstable periodics. **(C)** Periodic bursting corresponding to a torus canard with a head for $J = -32.92$ nA (note that this value is different from Fig. 14C). This solution features a similar change in drift to the headless canard but jumps down all the way to the lower branch of the Z-curve after it follows the unstable periodics. **(D)** Periodic bursting for $J = -30.0$ nA, which lacks an excursion along the branch of unstable periodics. (For interpretation of the references to color in this figure legend, the reader is referred to the web version of this article.)

the full system undergoes a torus bifurcation, which gives rise to spiking solutions that exhibit amplitude modulation across successive spikes. This modulation is initially small but then rapidly (with respect to parameter variation) grows in a torus canard explosion, eventually yielding a transition to bursting. Within the torus canard explosion, there are torus canard solutions, which pass from the attracting to the repelling branch of the fast subsystem periodic orbit manifold, across the SNPO. Existing theoretical work on torus canards has proceeded by averaging the fast subsystem dynamics and applying various principles of canard theory to the resulting averaged systems [5,84]; these works also developed certain reduced or canonical models that seem to capture the key transitions observed numerically. A rigorous connection of canard theory within an averaged system to the torus canard dynamics seen in simulations in the corresponding full system has not yet been established, although relevant results may be imminent [109].

5. Discussion

In this article we illustrate some dynamical systems methods by which one can take advantage of well-separated timescales to analyze multi-timescale systems and thereby elucidate the dynamic mechanisms underlying the solutions that they generate. As we

have presented, a variety of such methods exist that apply once the classification of the timescales on which the dynamic components evolve has been established. These methods generally proceed by focusing on fast and slow dynamics sequentially, with an initial identification of fast subsystem attractors followed by an evaluation of how slow dynamics can sweep the system along or between these attractors. The consideration of slow dynamics, with faster variables slaved to the slow ones via some sort of rapid convergence to an equilibrium, is analogous to the quasi-steady state approach that commonly is applied in the analysis of biochemical reactions and other biological systems [11,12,43,90]. We have also seen some instances, such as with canards and mixed-mode oscillations, when the separation of timescales can break down along a trajectory, even though the fast and slow timescales in the underlying dynamical system appear to be well separated, and unexpected solution behaviors can result.

Of course, there are a range of other types of multiple-timescale dynamics and analysis that have appeared in the literature or are in need of future attention. For example, within the general area of bursting, an entire book was published about 10 years ago on topics that go beyond the fundamental bifurcation-based burst classifications [24], and many other examples have appeared since then. A few examples of related areas include bursting dynamics that

involve more than the usual two (active-to-silent and silent-to-active) fast subsystem bifurcations per cycle (e.g., [89]), burst dynamics in stochastic systems (e.g., [21,26,46,59,73,97]), analysis of the phase-dependence of how bursting systems respond to forcing (e.g., [18,27,92]), and map-based representations of bursting dynamics (reviewed in [49]). Fast-slow analysis along the lines of what we have presented has been used to analyze multi-stability of bursting solutions for fixed parameter values [17,19,20], while other authors have considered how bistability between bursting and spiking dynamics can arise (e.g., [93]).

While methods of fast-slow analysis have proven quite useful in a wide variety of analyses, the reality is that, when modeling a biological system in practice, it may not be evident how many timescales are needed to capture observed dynamics. Similarly, once a model has been constructed, with parameter values determined based on biological principles or parameter estimation methods, it may turn out that the timescales of some of the model variables are not so well separated, and in some cases it may not be clear how to partition the variables into timescale classes. In addressing such questions, it is useful to recognize the importance of nondimensionalization [60]. Naturally, the same timescale parameter can appear to be much larger or smaller depending on the units in which it is expressed. Nondimensionalization removes this arbitrariness, providing unitless parameter groupings and illuminating the effective timescales that are present. Nonetheless, even after this step, judgments will be needed about when differences in time constants truly represent distinct timescales. As a starting point, numerical experimentation can be used to check whether model dynamics changes qualitatively as time constants of certain variables are pushed apart, in which case these variables should probably be considered as evolving on the same timescale. Unfortunately, this process may be less precise than one would desire; however, if it can be complemented by an analysis (e.g., using the fast-slow techniques that we have surveyed) of the dynamic mechanisms involved in producing solution behavior and in changing it as parameters are varied, then a more definitive assessment of timescale separation can be made (e.g., [69]).

One interesting case arises when certain variables evolve on intermediate timescales, relative to the more extreme fast and slow timescales in a system. How one partitions the variables into subsystems will in general determine the type of information that can be extracted from the analysis. For example, in [107] a 4-variable model for the electrical activity of a pituitary cell was analyzed using several different partitions of the variables. The traditional approach is to treat the slowest variable as "slow" and the remaining three variables as "fast", as we presented in our discussion of bursting dynamics. With this splitting one is able to study transitions between active and silent phases of a burst, but the mechanism for the spiking that occurs during a burst is not resolved, and neither is the boundary in parameter space between a spiking solution and a bursting solution. At the opposite extreme, one treats the fastest variable as "fast" and the remaining three as "slow". Now the dynamics of the full system are interpreted in terms of a folded critical manifold and canard orbits, which are the basis of the small spikes in the so-called pseudo-plateau bursting exhibited by pituitary cells. The limitation now is that the 3-dimensional slow subsystem is hard to work with, and by treating 3 of the 4 variables as slow one is not taking advantage of timescale differences that could exist between these three variables. The best approach, as demonstrated in [107], is to partition the variables into 3 distinct timescales; one variable is "fast", two variables are "intermediate", and the slowest variable is "slow". Now the 3-dimensional critical manifold of the 1-fast/3-slow splitting becomes a 2-dimensional critical manifold, which is simpler to work with. Also, canards are retained, and form the basis for the small spikes that occur during a pseudo-plateau burst. Most importantly,

the 1-fast/2-intermediate/1-slow splitting provides the resolution to analyze the spiking or bursting orbit during all phases of the trajectory. We anticipate that 3-timescale splittings will be a focus of theoretical and applied multi-timescale analyses in the near future, extending what has been done thus far [25,52,56,57,69,107].

If the 3-timescale decomposition provides more information than a 2-timescale splitting, why not partition into 4 distinct classes? In fact, the number of timescales that are necessary or useful for understanding system behavior depends on the system and on the features of the behavior in question. Direct inspection of time course data collected from a biological system, or model of that system, may be misleading in this regard. For example, the output of mammalian respiratory central pattern generator circuits can include patterns involving sequences of bursts of one type followed by a qualitatively different type of burst, such as sighing patterns in which a sequence of usual respiratory bursts is interrupted by a prolonged sigh-burst. These patterns seem like they should involve 3-timescale dynamics comprising fast and slow components that produce the basic bursting rhythm along with a superslow component that gradually allows the system to progress to the point where it produces its altered output, such as the sigh. While 3-timescale models can produce both patterns [36,53,72,99,100], careful analysis involving nondimensionalization, timescale decomposition, bifurcation analysis, and direct simulations shows that certain mixed bursting patterns of this type can be produced with just two timescales, while the sighing patterns truly do require 3 timescales, at least in these models [110,111]. In the 2-timescale case, no significant additional information is gained by a partition into 3 timescales. The good news is that the methods that we have surveyed, and related extensions, equip us with the tools to make these types of evaluations and thereby elucidate the mechanisms underlying multi-timescale biological dynamics, explain transitions between different solution behaviors under variation of system parameters, and make informed predictions for subsequent biological testing.

Acknowledgments

References

[1] F.M. Ashcroft, D.E. Harrison, S.J.H. Ashcroft, Glucose induces closure of single potassium channels in isolated rat pancreatic β-cells, Nature 312 (1984) 446–448.

[2] S.M. Baer, T. Erneux, Singular hopf bifurcation to relaxation oscillations, SIAM J. Appl. Math. 46 (1986) 721–739.

[3] S.M. Baer, T. Erneux, Singular hopf bifurcation to relaxation oscillations II, SIAM J. Appl. Math. 52 (1992) 1651–1664.

[4] S.M. Baer, J. Rinzel, H. Carrillo, Analysis of an autonomous phase model for neuronal parabolic bursting, J. Math. Biol. 33 (1995) 309–333.

[5] G. Benes, A. Barry, T. Kaper, M. Kramer, J. Burke, An elementary model of torus canards, Chaos 21 (2) (2011) 023131.

[6] E. Benoit, Syst'emes lents-rapids dans r3 et leur canards, Asterique 109–110 (1983) 159–191.

[7] R. Bertram, M.J. Butte, T. Kiemel, A. Sherman, Topological and phenomenological classification of bursting oscillations, Bull. Math. Biol. 57 (1995) 413–439.

[8] R. Bertram, J. Previte, A. Sherman, R.A. Kinard, L.S. Satin, The phantom burster model for pancreatic β-cells, Biophys. J. 79 (2001) 2880–2892.

[9] J. Best, A. Borisyuk, J. Rubin, D. Terman, M. Wechselberger, The dynamic range of bursting in a model respiratory pacemaker network, SIAM J. Appl. Dyn. Syst. 4 (2005) 1107–1139.

[10] G. Boehmer, W. Greffrath, E. Martin, S. Hermann, Subthreshold oscillation of the membrane potential in magnocellular neurones of the rat supraoptic nucleus, J. Physiol. 526 (2000) 115–128.

[11] J. Borghans, R. DeBoer, L. Segel, Extending the quasi-steady state approximation by changing variables, Bull. Math. Biol. 58 (1996) 43–63.

[12] G. Briggs, J. Haldane, A note on the kinetics of enzyme action, Biochem. J. 19 (1925) 338–339.

[13] M. Brøns, K. Bar-Eli, Canard explosion and excitation in a model of the Belousov-Zhabotinsky reaction, J. Phys. Chem. 95 (1991) 8706–8713.

[14] M. Brøns, M. Krupa, M. Wechselberger, Mixed mode oscillations due to the generalized canard phenomenon, Fields Inst. Commun. 49 (2006) 39–63.

[15] J. Burke, M. Desroches, A. Barry, T. Kaper, M. Kramer, A showcase of torus canards in neuronal bursters, J. Math. Neurosci. 2 (1) (2012) 1–30.

[16] R. Butera Jr, J. Clark Jr, J.H. Byrne, Transient responses of a modeled bursting neuron: analysis with equilibrium and averaged nullclines, Biol. Cybern. 77 (5) (1997) 307–322.

[17] R.J. Butera Jr, Multirhythmic bursting, Chaos 8 (1) (1998) 274–284.

[18] C. Canavier, Analysis of circuits containing bursting neurons using phase resetting curves, in: S. Coombes, P. Bressloff (Eds.), Bursting: the genesis of rhythm in the nervous system, World Scientific, 2005, pp. 175–200.

[19] C. Canavier, D. Baxter, J. Clark, J. Byrne, Nonlinear dynamics in a model neuron provide a novel mechanism for transient synaptic inputs to produce long-term alterations of postsynaptic activity, J. Neurophysiol. 69 (6) (1993) 2252–2257.

[20] C. Canavier, D. Baxter, J. Clark, J. Byrne, Multiple modes of activity in a model neuron suggest a novel mechanism for the effects of neuromodulators, J. Neurophysiol. 72 (2) (1994) 872–882.

[21] P. Channell, I. Fuwape, A.B. Neiman, A.L. Shilnikov, Variability of bursting patterns in a neuron model in the presence of noise, J. Comput. Neurosci. 27 (3) (2009) 527–542.

[22] T.R. Chay, J. Keizer, Minimal model for membrane oscillations in the pancreatic β-cell, Biophys. J. 42 (1983) 181–190.

[23] D.L. Cook, L.S. Satin, M.J. Ashford, C.N.H. s, ATP-sensitive K^+ channels in pancreatic β–cells: spare–channel hypothesis, Diabetes 37 (1988) 495–498.

[24] S. Coombes, P.C. Bressloff, Bursting: The Genesis of Rhythm in the Nervous System, World Scientific Press, Singapore, 2005.

[25] P. De Maesschalck, E. Kutafina, N. Popović, Three time-scales in an extended Bonhoeffer–van der Pol oscillator, J. Dyn. Differ. Equ. 26 (4) (2014) 955–987.

[26] G. De Vries, A. Sherman, Channel sharing in pancreatic β-cells revisited: enhancement of emergent bursting by noise, J. Theor. Biol. 207 (4) (2000) 513–530.

[27] S. Demir, R. Butera Jr, A. DeFranceschi, J. Clark Jr, J. Byrne, Phase sensitivity and entrainment in a modeled bursting neuron, Biophys. J. 72 (2 Pt 1) (1997) 579.

[28] M. Desroches, J. Burke, T. Kaper, M. Kramer, Canards of mixed type in a neural burster, Phys. Rev. E 85 (2012) 021920.

[29] M. Desroches, J. Guckenheimer, B. Krauskopf, C. Kuehn, H.M. Osinga, M. Wechselberger, Mixed-mode oscillations with multiple time scales, SIAM Rev. 54 (2012) 211–288.

[30] C.T. Dickson, J. Magistretti, M. Shalinsky, B. Hamam, A. Alonso, Oscillatory activity in entorhinal neurons and circuits. Mechanisms and function, Ann. N.Y. Acad. Sci. 911 (2000) 127–150.

[31] M. Diener, The canard unchained or how fast/slow dynamical systems bifurcate, Math. Intell. 6 (1984) 38–48.

[32] S. Doi, S. Nabetani, S. Kumagai, Complex nonlinear dynamics of the Hodgkin-Huxley equations, Biol. Cybern. 85 (2001) 51–64.

[33] J. Drover, J. Rubin, J. Su, B. Ermentrout, Analysis of a canard mechanism by which excitatory synaptic coupling can synchronize neurons at low firing frequencies, SIAM J. Appl. Math. 65 (2004) 69–92.

[34] W. Duan, K. Lee, A.E. Herbison, J. Sneyd, A mathematical model of adult GnRH neurons in mouse brain and its bifurcation analysis, J. Theor. Biol. 276 (2011) 22–34.

[35] F. Dumortier, R. Roussarie, Canard cycles and center manifolds, Mem. Am. Math. Soc. 121 (1996) 1–100.

[36] J.R. Dunmyre, C.A. Del Negro, J.E. Rubin, Interactions of persistent sodium and calcium-activated nonspecific cationic currents yield dynamically distinct bursting regimes in a model of respiratory neurons, J. Comput. Neurosci. 31 (2) (2011) 305–328.

[37] W. Eckhaus, Relaxation oscillations including a standard chase on French ducks, in: F. Verhulst (Ed.), Asymptotic analysis II, Lecture Notes in Mathematics, vol. 985, Springer, Berlin, 1983, pp. 449–494.

[38] G.B. Ermentrout, D.H. Terman, Mathematical Foundations of Neuroscience, vol. 35, Springer Science & Business Media, 2010.

[39] N. Fenichel, Geometric singular perturbation theory for ordinary differential equations, J. Differ. Equ. 31 (1) (1979) 53–98.

[40] R. FitzHugh, Impulses and physiological states in theoretical models of nerve membrane, Biophys. J. 1 (1961) 445–466.

[41] R. FitzHugh, An active pulse transmission line simulating nerve axon, Proc. IRE 50 (1962) 2061–2070.

[42] J. Grasman, Asymptotic methods for relaxation oscillations and applications, Springer, New York, NY, 1987.

[43] J. Gunawardena, Time-scale separation–Michaelis and Menten's old idea, still bearing fruit, FEBS J. 281 (2) (2014) 473–488.

[44] Y. Gutfreund, Y. Yarom, I. Segev, Subthreshold oscillations and resonant frequency in guinea-pig cortical neurons: physiology and modelling, J. Physiol. 483 (1995) 621–640.

[45] E. Harvey, V. Kirk, M. Wechselberger, J. Sneyd, Multiple timescales, mixed mode oscillations and canards in models of intracellular calcium dynamics, J. Nonlinear Sci. 21 (2011) 639–683.

[46] P. Hitczenko, G.S. Medvedev, Bursting oscillations induced by small noise, SIAM J. Appl. Math. 69 (5) (2009) 1359–1392.

[47] A.L. Hodgkin, A.F. Huxley, A quantitative description of membrane current and its application to conduction and excitation in nerve, J. Physiol. 117 (4) (1952) 500.

[48] M.H. Holmes, Introduction to perturbation methods, Springer, New York, NY, 2013.

[49] B. Ibarz, J.M. Casado, M.A. Sanjuán, Map-based models in neuronal dynamics, Phys. Rep. 501 (1) (2011) 1–74.

[50] C. Iglesias, C. Meunier, M. Manuel, Y. Timofeeva, N. Delestrée, D. Zytnicki, Mixed mode oscillations in mouse spinal motorneurons arise from a low excitability state, J. Neurosci. 31 (2011) 5829–5840.

[51] E.M. Izhikevich, Neural excitability, spiking, and bursting, Int. J. Bifur. Chaos 10 (2000) 1171–1266.

[52] J. Jalics, M. Krupa, H.G. Rotstein, Mixed-mode oscillations in a three time-scale system of ODEs motivated by a neuronal model, Dyn. Syst. 25 (2010) 445–482.

[53] P. Jasinski, Y. Molkov, N. Shevtsova, J. Smith, I. Rybak, Sodium and calcium mechanisms of rhythmic bursting in excitatory neural networks of the pre-Bötzinger complex: a computational modelling study, Eur. J. Neurosci. 37 (2) (2013) 212–230.

[54] M.A. Kramer, R.D. Traub, N.J. Kopell, New dynamics in cerebellar purkinje cells: torus canards, Phys. Rev. Lett. 101 (2008) 068103–1–068103–4.

[55] K. Krischer, M. Eiswirth, G. Ertl, Oscillatory CO oxidation on Pt(110): modeling of temporal self-organization, J. Chem. Phys. 96 (1992), doi:10.1063/1.462226.

[56] M. Krupa, N. Popović, N. Kopell, Mixed-mode oscillations in three time-scale systems: a prototypical example, SIAM J. Appl. Dyn. Syst. 7 (2008) 361–420.

[57] M. Krupa, N. Popović, N. Kopell, H.G. Rotstein, Mixed-mode oscillations in a three time-scale model for the dopaminergic neuron, Chaos 18 (2008) 015106

[58] M. Krupa, P. Szmolyan, Relaxation oscillation and canard explosion, J. Differ. Equ. 174 (2001) 312–368.

[59] R. Kuske, S. Baer, Asymptotic analysis of noise sensitivity in a neuronal burster, Bull. Math. Biol. 64 (3) (2002) 447–481.

[60] C. Lin, L. Segel, Mathematics Applied to Deterministic Problems in the Natural Sciences, SIAM, Philadelphia, PA, 1988.

[61] J.E. Lisman, Bursts as a unit of neural information: making unreliable synapses reliable, Trends Neurosci. 20 (1997) 38–43.

[62] R.R. Llinás, A.A. Grace, Y. Yarom, In vitro neurons in mammalian cortical layer 4 exhibit intrinsic oscillatory activity in the 10- to 50-Hz frequency range, Proc. Natl. Acad. Sci. USA 88 (1991) 897–901.

[63] P.A. Mathieu, F.A. Roberge, Characteristics of pacemaker oscillations in Aplysia neurons, Can. J. Physiol. Pharmacol. 49 (1971) 787–795.

[64] J.P. McKenna, J. Ha, M.J. Merrins, L.S. Satin, A. Sherman, R. Bertram, Ca^{2+} effects on ATP production and consumption have regulatory roles on oscillatory islet activity, Biophys. J. 110 (2016) 733–742.

[65] G.S. Medvedev, J.E. Cisterna, Multimodal regimes in a compartmental model of the dopamine neuron, Physica D 194 (2004) 333–356.

[66] M.J. Merrins, C. Poudel, J.P. McKenna, J. Ha, A. Sherman, R. Bertram, L.S. Satin, Phase analysis of metabolic oscillations and membrane potential in pancreatic β cells, Biophys. J. 110 (2016) 691–699.

[67] M. Mikikian, M. Cavarroc, L. Couëdel, Y. Tessier, L. Boufendi, Mixed-mode oscillations in complex-plasma instabilities, Phys. Rev. Lett. 100 (2008), doi:10.1103/PhysRevLett.100.225005.

[68] C. Morris, H. Lecar, Voltage oscillations in the barnacle giant muscle fiber, Biophys. J. 35 (1981) 193–213.

[69] P. Nan, Y. Wang, V. Kirk, J.E. Rubin, Understanding and distinguishing three–time-scale oscillations: case study in a coupled Morris–Lecar system, SIAM J. Appl. Dyn. Syst. 14 (3) (2015) 1518–1557.

[70] C.S. Nunemaker, R. Bertram, A. Sherman, K. Tsaneva-Atanasova, C.R. Daniel, L.S. Satin, Glucose modulates $[Ca^{2+}]_i$ oscillations in pancreatic islets via ionic and glyoclytic mechanisms, Biophys. J. 91 (2003) 2082–2096.

[71] M.J. O'Donovan, The origin of spontaneous activity in developing networks of the vertebrate nervous system, Curr. Opin. Neurobiol. 9 (1999) 94–104.

[72] C. Park, J.E. Rubin, Cooperation of intrinsic bursting and calcium oscillations underlying activity patterns of model pre-Bötzinger complex neurons, J. Comp. Neurosci. 34 (2) (2013) 345–366.

[73] M.G. Pedersen, M.P. Sørensen, The effect of noise on β-cell burst period, SIAM J. Appl. Math. 67 (2) (2007) 530–542.

[74] C. Perryman, S. Wieczorek, Adapting to a changing environment: non-obvious thresholds in multi-scale systems, Proc. R. Soc. A 470 (2170) (2014) 20140226.

[75] V. Petrov, S.K. Scott, K. Showalter, Mixed-mode oscillations in chemical systems, J. Chem. Phys. 97 (1992) 6191–6198.

[76] R.E. Plant, Bifurcation and resonance in a model for bursting nerve cells, J. Math. Biol. 11 (1981) 15–32.

[77] S. Rinaldi, M. Scheffer, Geometric analysis of ecological models with slow and fast processes, Ecosystems 3 (6) (2000) 507–521.

[78] J. Rinzel, Bursting oscillations in an excitable membrane model, in: B.D. Sleeman, R.J. Jarvis (Eds.), Ordinary and Partial Differential Equations, Lecture Notes in Mathematics, vol. 1151, Springer, Berlin, 1985, pp. 304–316.

[79] J. Rinzel, A formal classification of bursting mechanisms in excitable systems, in: E. Teramoto, M. Yamaguti (Eds.), Mathematical topics in population biology, morphogenesis and neurosciences, Lecture Notes in Biomathematics, vol. 71, Springer-Verlag, Berlin, 1987, pp. 267–281.

[80] J. Rinzel, G.B. Ermentrout, Analysis of neural excitability and oscillations, in: C. Koch, I. Segev (Eds.), Methods in Neuronal Modeling: From Synapses to Networks (2nd Edition), MIT Press, Cambridge, 1998, pp. 251–292.

[81] J. Rinzel, Y. Lee, On different mechanisms for membrane potential bursting, in: H. Othmer (Ed.), Nonlinear Oscillations in Biology and Chemistry, Lecture Notes in Biomathematics, vol. 66, Springer, New York, 1986, pp. 19–33.

[82] J. Rinzel, Y.S. Lee, On different mechanisms for membrane potential bursting, in: H.G. Othmer (Ed.), Nonlinear Oscillations in Biology and Chemistry, Lecture Notes in Biomathematics, vol. 66, Springer–Verlag, Berlin, 1985, pp. 19–33.

[83] J. Rinzel, Y.S. Lee, Dissection of a model for neuronal parabolic bursting, J. Math. Biol. 25 (1987) 653–675.

[84] K.-L. Roberts, J. Rubin, M. Wechselberger, Averaging, folded singularities and torus canards: explaining transitions between bursting and spiking in a coupled neuron model, SIAM J. Appl. Dyn. Syst. 14 (4) (2015) 1808–1844.

[85] H.G. Rotstein, T. Oppermann, J.A. White, N. Kopell, The dynamic structure underlying subthreshold activity and the onset of spikes in a model of medial entorhinal cortex stellate cells, J. Comput. Neurosci. 21 (2006) 271–292.

[86] H.G. Rotstein, M. Wechselberger, N. Kopell, Canard induced mixed-mode oscillations in a medial entorhinal cortex layer II stellate cell model, SIAM J. Appl. Dyn. Syst. 7 (2008) 1582–1611.

[87] J. Rubin, M. Wechselberger, Giant squid-hidden canard: the 3D geometry of the Hodgkin-Huxley model, Biol. Cybern. 97 (2007) 5–32.

[88] J. Rubin, M. Wechselberger, The selection of mixed-mode oscillations in a Hodgkin-Huxley model with multiple timescales, Chaos 18 (1) (2008) 015105.

[89] J.E. Rubin, J.A. Hayes, J.L. Mendenhall, C.A. Del Negro, Calcium-activated nonspecific cation current and synaptic depression promote network-dependent burst oscillations, Proc. Natl. Acad. Sci. USA 106 (8) (2009) 2939–2944.

[90] L.A. Segel, M. Slemrod, The quasi-steady-state assumption: a case study in perturbation, SIAM Rev. 31 (3) (1989) 446–477.

[91] A. Sherman, Contributions of modeling to understanding stimulus-secretion coupling in pancreatic β-cells, Am. J. Physiol. 271 (1996) E362–E372.

[92] W.E. Sherwood, J. Guckenheimer, Dissecting the phase response of a model bursting neuron, SIAM J. Appl. Dyn. Syst. 9 (3) (2010) 659–703.

[93] A. Shilnikov, R.L. Calabrese, G. Cymbalyuk, Mechanism of bistability: tonic spiking and bursting in a neuron model, Phys. Rev. E 71 (5) (2005) 056214.

[94] P. Smolen, D. Terman, J. Rinzel, Properties of a bursting model with two slow inhibitory variables, SIAM J. Appl. Math. 53 (3) (1993) 861–892.

[95] S.S. Stojilkovic, J. Tabak, R. Bertram, Ion channels and signaling in the pituitary gland, Endocr. Rev. 31 (2010) 845–915.

[96] J.J. Stoker, Nonlinear vibrations in mechanical and electrical systems, Wiley-Interscience, New York, NY, 1992.

[97] J. Su, J. Rubin, D. Terman, Effects of noise on elliptic bursters, Nonlinearity 17 (1) (2003) 133.

[98] J. Tabak, J. Rinzel, M.J. O'Donovan, The role of activity-dependent network depression in the expression and self-regulation of spontaneous activity in the developing spinal cord, J. Neurosci. 21 (2001) 8966–8978.

[99] N. Toporikova, R.J. Butera, Two types of independent bursting mechanisms in inspiratory neurons: an integrative model, J. Comput. Neurosci. 30 (3) (2011) 515–528.

[100] N. Toporikova, M. Chevalier, M. Thoby-Brisson, Sigh and eupnea rhythmogenesis involve distinct interconnected subpopulations: a combined computational and experimental study, eNeuro 2 (2) (2015) ENEURO–0074.

[101] B. Van der Pol, Lxxxviii. on relaxation-oscillations, London Edinb. Dublin Philos. Mag. J. Sci. 2 (11) (1926) 978–992.

[102] B. van der Pol, On relaxation-oscillations, Phil. Mag. 7 (1926) 978–992.

[103] B. van der Pol, J. van der Mark, The heartbeat considered as a relaxation oscillation, and an electrical model of the heart, Phil. Mag. 6 (1928) 763–775.

[104] F. Van Goor, D. Zivadinovic, A.J. Martinez-Fuentes, S.S. Stojilkovic, Dependence of pituitary hormone secretion on the pattern of spontaneous voltage-gated calcium influx, J. Biol. Chem. 276 (2001) 33840–33846.

[105] A. Vidal, F. Clément, A dynamical model for the control of the gonadotropin-releasing hormone neurosecretory system, J. Neuroendocrinol. 22 (2010) 1251–1266.

[106] T. Vo, R. Bertram, J. Tabak, M. Wechselberger, Mixed mode oscillations as a mechanism for pseudo-plateau bursting, J. Comput. Neurosci. 28 (2010) 443–458.

[107] T. Vo, R. Bertram, M. Wechselberger, Multiple geometric viewpoints of mixed mode dynamics associated with pseudo-plateau bursting, SIAM J. Appl. Dyn. Syst. 12 (2013) 789–830.

[108] T. Vo, J. Tabak, R. Bertram, M. Wechselberger, A geometric understanding of how fast activating potassium channels promote bursting in pituitary cells, J. Comput. Neurosci. 36 (2014) 259–278.

[109] T. Vo, M. Wechselberger, Canards of folded saddle-node type I, SIAM J. Math. Anal. 47 (4) (2015) 3235–3283.

[110] Y. Wang, Analysis of complex bursting patterns in multiple time scale respiratory neuron models, Ph.D. dissertation, University of Pittsburgh (2016).

[111] Y. Wang, Multiple timescale mixed bursting dynamics in a respiratory neuron model, J. Comput. Neurosci. (2016), doi:10.1007/s10827-016-0616-6.

[112] M. Watts, J. Tabak, C. Zimliki, A. Sherman, R. Bertram, Slow variable dominance and phase resetting in phantom bursting, J. Theor. Biol. 276 (2011) 218–228.

[113] M. Wechselberger, Existence and bifurcation of canards in $\mathbb{R}^3$ in the case of a folded node, SIAM J. Appl. Dyn. Syst. 4 (1) (2005) 101–139.

[114] M. Wechselberger, A propos de canards (apropos canards), Trans. Am. Math. Soc. 364 (6) (2012) 3289–3309.